Brain, Behavior, and Immunity 77 (2019) 110–126

Contents lists available at ScienceDirect

Brain, Behavior, and Immunity

journal homepage: www.elsevier.com/locate/ybrbi

Full-length Article

The endocannabinoid 2-AG enhances spontaneous remyelination by targeting microglia

M. Mecha[a,*,1], N. Yanguas-Casás[a,b,1], A. Feliú[a], L. Mestre[a], F. Carrillo-Salinas[a,2], I. Azcoitia[b,c], V.W. Yong[d], C. Guaza[a,*]

[a] Departamento de Neurobiología Funcional y de Sistemas, Grupo de Neuroinmunología, Instituto Cajal, CSIC, Spain
[b] CIBER de Investigación Biomédica en Red de Fragilidad y Envejecimiento Saludable (CIBERFES), Instituto de Salud Carlos III, Madrid, Spain
[c] Departamento de Biología Celular, Facultad de Biología, Universidad Complutense, Madrid 28040, Spain
[d] Hotchkiss Brain Institute, and the Departments of Clinical Neurosciences and Oncology, University of Calgary, 3330 Hospital Drive, Calgary, Alberta T2N 4N1, Canada

ARTICLE INFO

Keywords:
Remyelination
Endocannabinoids
Microglia
Phagocytosis
TMEV

ABSTRACT

Remyelination is an endogenous process by which functional recovery of damaged neurons is achieved by re-instating the myelin sheath around axons. Remyelination has been documented in multiple sclerosis (MS) lesions and experimental models, although it is often incomplete or fails to affect the integrity of the axon, thereby leading to progressive disability. Microglia play a crucial role in the clearance of the myelin debris produced by demyelination and in inflammation-dependent OPC activation, two processes necessary for remyelination to occur. We show here that following corpus callosum demyelination in the TMEV-IDD viral murine model of MS, there is spontaneous and partial remyelination that involves a temporal discordance between OPC mobilization and microglia activation. Pharmacological treatment with the endocannabinoid 2-AG enhances the clearance of myelin debris by microglia and OPC differentiation, resulting in complete remyelination and a thickening of the myelin sheath. These results highlight the importance of targeting microglia during the repair processes in order to enhance remyelination.

1. Introduction

In the adult CNS, the loss of myelin is characteristic of demyelinating diseases like multiple sclerosis (MS), although it is often followed by a spontaneous process of remyelination, whereby oligodendrocyte progenitor cells (OPCs) differentiate and synthesize myelin to ensheath the exposed axons (Chari, 2007). A hallmark of the remyelination in MS is the so-called shadow plaques, where myelin staining lies is interspersed between the demyelinated plaques and the normal white matter (Prineas et al., 1993; Plemel et al., 2017). However, the myelin sheaths generated during remyelination are typically shorter and thinner than those generated during normal development (Blakemore, 1974; Ludwin and Maitland, 1984).

The remyelination of axons not only restores saltatory conduction but it also favors neuronal survival (Chari and Blakemore, 2002; Nave, 2010). Therefore, strategies designed to enhance this endogenous mechanism of repair are likely to be neuroprotective, limiting the clinical disability associated with degeneration in demyelinating diseases. Although OPCs can be found in most chronically demyelinated MS lesions, they have become quiescent and are unable to differentiate (Plemel et al., 2017), or their maturation is frozen in a premyelinating state in which the oligodendrocytes contact and ensheath the axons but without forming compact myelin (Chang et al., 2002). For remyelination to occur, the intrinsic factors in OPCs must be orchestrated with the extrinsic signaling associated with OPC proliferation, migration and differentiation, driving processes that include the inflammation-

Abbreviations: AEA, anandamide; 2-AG, 2-arachidonoylglycerol; Arg-1, arginase-1; CB, cannabinoid; CCL2, chemokine (C–C) ligand 2; CNS, central nervous system; DAGLs, diacylglycerol lipases; dpi, days post-infection; eCBs, endocannabinoids; EAE, experimental autoimmune encephalomyelitis; FCS, fetal calf serum; IL-1β, interleukin-1β; IL-10, interleukin-10; MS, multiple sclerosis; MBP, Myelin Basic Protein; NOS-II, inducible nitric oxide synthase type II; MAGL, monoacylglycerol lipase; OPC, oligodendrocyte precursor cell; PFA, paraformaldehyde; TMEV-IDD, Theiler's murine encephalomyelitis virus-induced demyelinating disease; TNFα, tumor necrosis factor α

* Corresponding authors at: Grupo de Neuroinmunología, Instituto Cajal, CSIC, Madrid, Spain.
E-mail addresses: miriammecha@cajal.csic.es (M. Mecha), cgjb@cajal.csic.es (C. Guaza).
[1] These authors contributed equally to this work.
[2] Present address: Sackler School of Graduate Biomedical Sciences, Tufts University School of Medicine, Boston, MA, USA.

https://doi.org/10.1016/j.bbi.2018.12.013
Received 26 June 2018; Received in revised form 19 December 2018; Accepted 20 December 2018
Available online 21 December 2018

dependent activation of OPCs (Miron et al., 2011) and the clearance of myelin debris by phagocytes (Kotter et al., 2005; Neumann et al., 2009; Lampron et al., 2015).

Microglia are thought to be detrimental in MS given their role in proinflammatory cytokine production, antigen presentation and autoimmunity (Fife et al., 2000; Heppner et al., 2005; Ajami et al., 2011). However, microglia may also have beneficial effects in remyelination since these cells might be associated with OPC recruitment and the phagocytosis of myelin debris during demyelination (Jurevics et al., 2002; Olah et al., 2012). Experimental models of demyelination have shown that the presence of myelin debris impairs CNS remyelination by inhibiting OPC differentiation (Kotter et al., 2006) and that efficient clearance of myelin by microglia is required for remyelination to occur (Lampron et al., 2015). Hence, microglia are pivotal cells in spontaneous CNS regeneration.

The Theiler's induced demyelinating disease model (TMEV-IDD) resembles MS pathogenesis in terms of inflammation, demyelination and neurodegeneration (Mecha et al., 2013a; Oleszak et al., 2004; Tsunoda and Fujinami, 2010). In this model, pharmacological treatment with synthetic cannabinoids, phytocannabinoids and even endocannabinoids (eCBs) exerts beneficial effects, limiting inflammation in the acute (Mestre et al., 2011; Mecha et al., 2013b, 2018) and chronic phase of the disease (Arévalo-Martín et al., 2003; Croxford and Miller 2003; Ortega-Gutiérrez et al., 2005; Feliú et al., 2015; Granja et al., 2012). In particular, exogenous 2-AG treatment modulates the neuroinflammatory response following TMEV infection (Mecha et al., 2018) and it ameliorates the outcome of EAE (experimental autoimmune encephalomyelitis; Lourbopoulos et al., 2011), a commonly used model of MS. Similarly, the increased endogenous 2-AG tone associated with the inhibition of the MAGL enzyme (which drives 2-AG degradation) exerts therapeutic effects, promoting remyelination in the spinal cord of TMEV-IDD mice (Feliú et al., 2017) and preventing demyelination in the EAE model (Bernal-Chico et al., 2015).

To study the mechanisms underlying spontaneous remyelination, we have taken advantage of the preclinical phase of the TMEV-IDD model where prominent demyelination is evident in the corpus callosum 35 days post-infection (dpi). This demyelination is followed by a spontaneous and incomplete process of remyelination at 60 dpi, which is subsequently lost with progression into the chronic phase of the disease (Mecha et al., 2013b). We found a temporal discordance between the OPC recruitment and microglial activation in the demyelinated corpus callosum. In addition, the eCB synthesis and hydrolysis machinery was diminished specifically in this area. Enhancing eCB tone through continuous 2-AG delivery before the onset of spontaneous remyelination in TMEV-infected mice elicited a pro-regenerative response that involves microglia activation, myelin debris phagocytosis enhancement, and OPC differentiation. Consequently, the myelin content in the corpus callosum was restored and the g-ratio of remyelinated axons decreased at 60 dpi. Indeed, 2-AG also improved the phagocytic capacity of human and rodent microglia *in vitro*. These results highlight the relevance of targeting microglia during remyelination to orchestrate the clearance of myelin debris and OPC differentiation in order to achieve endogenous CNS repair.

2. Materials & methods

2.1. Animals

TMEV-IDD susceptible SJL/J female mice were obtained from Envigo and maintained under standard conditions. Four-to-six week-old mice were intracerebrally inoculated in the right hemisphere with 2×10^6 plaque forming units (pfu) of the Daniels strain of TMEV diluted in 30 µl of DMEM (Dulbecco's Minimal Essential Medium) supplemented with 10% fetal calf serum (FCS; Lledó et al., 1999), studying 3–6 animals per experimental group. Sham operated mice received only 30 µl of DMEM supplemented with 10% FCS. All experiments were performed following the ARRIVE guidelines and in accordance with EU (Directive 2010/63/EU) and National (Royal Decree 53/2013 BOE No. 34 and Comunidad de Madrid: ES 280790000184) guidelines. The Ethics Committee on Animal Experimentation at the Instituto Cajal (CSIC) approved all the procedures described in this study (protocol number: 2013/03 CEEA-IC).

2.2. Pharmacological treatment

Mice were deeply anesthetized 28 days after TMEV infection and osmotic pumps were inserted into a small pocket under the skin of the back of the mice for subcutaneous delivery. Two models of Alzet pumps were used to deliver 2-AG (3.5 mg/kg, Tocris Bioscience) or the vehicle (50% DMSO/15% ethanol/35% PBS -phosphate buffered saline): model 1007D delivering 0.5 µl/h/ for 7 days; and model 1002 delivering 0.26 µl/h for 14 days. The pumps delivered their load over 7 days in the case of 28–35 dpi treatments to analyze demyelination at day 35, or over 14 days in the case of 28–42 dpi treatments to analyze remyelination at 42 or 60 dpi. In those mice maintained to 60 dpi, the pumps were removed once the treatment had finished at 42 dpi.

2.3. Immunohistochemistry

Mice were anesthetized with pentobarbital (Doletal, 50 mg/kg body weight, intraperitoneally – i.p.) and perfused transcardially with 0.9% saline. For immunohistochemistry studies, the brains were fixed overnight with 4% paraformaldehyde (PFA) in PBS and coronal vibratome sections (50 µm thick: Leica Microsystems) were obtained from the olfactory bulb to the beginning of the hippocampus. Slices were collected in cold De Olmos solution and stored at −20 °C. For immunohistochemistry, free-floating brain sections were washed three times for 10 min with PBS, incubated with PBS containing 0.1% Triton-X100 (Merck Millipore) and blocked for 1 h at room temperature in blocking buffer containing 0.1% Triton X-100 and 5% normal serum (Vector Laboratories). The sections were then incubated overnight at 4 °C with primary antibodies against the following proteins: Arg-1 (1:50; sc-18351, Santa Cruz Biotechnology); CC1 (1:200; OP80, Calbiochem), Iba-1 (1:1000; 019-19741, Wako); Myelin Basic Protein (MBP, 1:500; MAB382, Millipore); NOS-II (1:50; 610329 BD Transduction); Olig-2 (1:200; sc-48817, Santa Cruz Biotechnology); PLP (1:500; ab105784, Abcam). On the following day the sections were rinsed three times for 10 min with PBS containing 0.1% Triton X-100 and then incubated for 1 h with an Alexa Fluor-conjugated (1:500, Molecular Probes Inc) or biotinylated (Vector Laboratories) secondary antibody. For immunofluorescence, sections were rinsed three times for 10 min with PBS and mounted. In the case of PLP immunostaining with the chromogen 3,3′ diaminobenzidine tetrahydrochloride (DAB: Sigma-Aldrich), the sections were incubated for 1 h with a biotin-peroxidase complex (Vector Laboratories, CA, USA) and finally with DAB. After staining, the sections were dehydrated, cleared with xylene and coverslipped. In all cases, the specificity of staining was confirmed by omitting the primary antibody.

2.4. RNA extraction, reverse transcription and RT-PCR

Mice were anesthetized with pentobarbital (Doletal, 50 mg/kg body weight, i.p.) and perfused transcardially with 0.9% saline. For *in vivo* gene expression analysis, microdissection of the whole brain was performed in ice-cold PBS to isolate the corpus callosum and adjacent cerebral cortex. For *in vitro* studies, microglial cells were seeded at a density of 100,000 cells/cm^2 and lysed 6 h or 24 h after treatment with 2-AG (1 nM, Tocris Biosciences), a dose selected on the basis of our previous studies (Mecha et al., 2015). In another subset of experiments, microglia were treated with 2-AG (1 nM) for 24 h and lysed 6 h after the addition of purified myelin (2 µg/mL). In each case, total RNA was extracted using an RNeasy Lipid Tissue Mini Kit (Qiagen), treated with

Table 1
Rat primers.

Rat primers				
Gene	Accession #	Forward primer 5′–3′	Reverse primer 5′–3′	Amplicon size
LAMP1	NM_012857.2	AGAAGGCTCCACGCATTTGA	TGCAGCCTAACCACCATCAG	137
LAMP2	NM_017068.2	CAGGTGGTTTCCGTGTCTCG	TCCAGTATGATGGCGCTTGAG	216
CD206	NM_001106123.2	GGTTGGATTGAGGCCTGAAA	AACGTCCCTTTGTTTTGAACATC	66
MSR1	NM_001191939.1	TCGACTGGTTGATGGTAGCG	ATCCTAGACTCCGGCAGACA	128
Scarb1	NM_031541.1	AGTAAAAAGGGCTCGCAGGA	CTTCTGGGCCCTACAGCTTG	112
SIRP1a	NM_013016.2	ACCCAGATCCAGGACACAAA	GTGGACCATGTCCAGGTCAG	186
TREM2	NM_001106884.1	CCACGTGTTTGTCCTGTTGC	CAGTGCCTCAAGGCGTCATA	120
36B4	NM_022402.2	TTCCCACTGGCTGAAAAGGT	CGCAGCCGCAAATGC	60
RPS29	NM_012876.1	CTCGTTCCTTTTTCCTCCTTGG	TACTGACGGAAGCACTGTCG	174

Table 2
Mouse primers.

Mouse primers				
Gene	Accession #	Forward primer 5′-3′	Reverse primer 5′-3′	Amplicon size
Arg1	NM_007482.3	ATGGAAGAGACCTTCAGCTAG	GCTGTCTTCCCAAGAGTTGGG	224
CCL2	NM_011333.3	AGCAGGTGTCCCAAAGAAGCTGTA	AAAGGTGCTGAAGACCTTAGGGCA	176
CD47	NM_010581.3	CACGGCCCCCTTTTGATTTC	CTTCCAGCTGTGAGTCGTGA	137
IL1b	NM_008361.4	TGGTGTGTGACGTTCCCATT	TCCATTGAGGTGGAGAGCTTTC	110
IL10	NM_010548.2	TGAATTCCCTGGGTGAGAAGCTGA	TGGCCTTGTAGACACCTTGGTCTT	147
LAMP1	NM_001317353.1	AGCATACCGGTGTGTCAGTG	GGGAAGGTCCATCCTGTGTG	140
LAMP2	NM_010685.4	CTTAGCTTCTGGGATGCCCC	TCATCCAGCGAACACTCCTG	164
CD206	NM_008625.2	GGTTGGATTGAGGCCTGAAA	AACGTCCCTTTGTTTTGAACATC	66
MBP	NM_001025259.2	ACACACGAGAACTACCCATTATGG	AGAAATGGACTACTGGGTTTTCATCT	86
MSR1	NM_031195.2	CAGTGCTGTCTTCTTTACCAGC	CTGAAGGGAGGGGCCATTTT	167
NOS-II	NM_001313922.1	ACATTGATCTCCGTGACAGCC	CCCTTCAATGGTTGGTACATG	158
Olig2	NM_016967.2	GACTCCCCCCTCCGTCTAAG	CGCAGTAAAGCCCACGTTGT	147
PLP	NM_001290562.1 NM_001290561.1	CCCACCCCTATCCGCTAGTT	CAGGAAAAAAAGCACCATTGTG	71
SIRPα	NM_007547.4	ACCCAGATCCAGGACACAAA	GTGGACCATGTCCAGGTCAG	186
TNFα	NM_013693.3	AGAGGCACTCCCCCAAAAGA	CGATCACCCCGAAGTTCAGT	128
TREM2	NM_031254.3	GCACCTCCAGGAATCAAGAG	GGGTCCAGTGAGGATCTGAA	200
18S	NR_003278.3	ATGCTCTTAGCTGAGTGTCCCG	ATTCCTAGCTGCGGTATCCAGG	101
RPS29	NM_009093.2	GCCGCGTCTGCTCCAA	ACATGTTCAGCCCGTATTTGC	54
CXCL-12	NM_021704.3	CGGTTCTTCGAGAGCCACAT	TCCTTTGGGCTGTTGTGCTT	192
Sema3A	NM_001243072.1	CAGGCTGTGGAGTGGAGTG	GCCTGATGCAACCTTCTGGA	175
Sema3F	NM_001311151.1	TTAGACCCGTGTTGGTCAGC	GGTCCATGCCCTGACAAGAA	182
DAGLa	NM_198114.2	AGCCCTCCAAGCTCATCTCA	TCAAGGGGCTCAATAAG	240
DAGLb	NM_144915.3	AGCGACGACTTGGTGTTCC	GCGTGAGATACAACGTCAGACT	85
MAGL	NM_001166251.1	ACTTGGAAGTCCGACACCAC	GGCGAACTCCACAGAATGTT	262
NAPE-PLD	NM_178728.6	ATGGTGGAAATGGACGAGCTCATC	TCATGTTTCTTCAAAAGCTCTATC	286
FAAH	NM_010173.5	TGGGCCCTGCTCTGGATTTG	CAGAGCTGGCGAATGAACGAC	340
IGF-1	NM_010512.5	GTGATCTGAGGAGACTGGAGATGTACT	TGAGTCTTGGGCATGTCAGTGT	100
BDNF	NM_007540.4	TCATACTTGGTTGCATGAAGG	AGACCTCTCGAACCTGCCC	137
	NM_001291058.1	TCTCTCATTTCCTTATGGACAGCTT	ATTGATTCCACCGCCATGTAGTC	99
MFG-E8	NM_008594.2	GAATACATCTGCCAGTGCCC	AGAACAACGGGAGGCTAGGTT	171

DNaseI (Promega) and 1 μg of this RNA was reverse transcribed using the High capacity cDNA reverse transcription kit (Applied Biosystems). The cDNA obtained was amplified by real-time PCR in a 7500 Real Time PCR System (Applied Biosystems) with the Power SYBR® Green reagent (Applied Biosystems). Gene expression was determined with 7500 Software v2.0.4 using ROX as a passive reference dye and represented using the comparative Ct (cycle threshold) method. The ΔCt was calculated by the difference between the Ct of each target gene and the Ct of an artificial BestKeeper reference gene based on the Ct values of two independent reference genes: RPS29/18S for *in vivo* analysis, and 36B4/RPS29 for *in vitro* studies (calculated using the BestKeeper© Software, http://gene-quantification.com/bestkeeper.html). We determined the mRNA expression of the set of genes listed in Tables 1 and 2.

2.5. Myelin purification and labeling

Myelin from 9-week old Wistar rat brains was isolated by sequential centrifugation on a discontinuous sucrose gradient, as described previously (Larocca and Norton, 2007). Briefly, 2 g of rat brain tissue was mechanically disaggregated in a 0.3 M sucrose solution, and layered on a sucrose gradient composed of 0.3 M and 0.83 M sucrose. Sequential ultracentrifugation was performed at 4 °C using a Thermo Scientific SureSpin 630 Rotor: 75,000 g, 30 min; 75,000 g, 15 min; and 12,000 g, 15 min. After two rounds of hypo-osmotic shock with a Tris-HCl buffer solution, the myelin was resuspended in sodium carbonate buffer (0.1 M $NaHCO_3$–Na_2CO_3, pH 9.4: Southwick et al., 1990) and stored at −80 °C. The myelin protein content was determined by the Bradford method, using bovine serum albumin as a standard, and 1 mg/ml myelin was labeled using CyTM3 (Mono-Reactive Dye Pack: Amersham Biosciences) according to the manufacturer's instructions, storing the Cy3 conjugated myelin at 4 °C.

2.6. Human microglia cultures

Adult human brain microglia ($Iba1^+$, > 95% purity) were obtained from brain specimens resected from patients that underwent surgery to treat intractable epilepsy and they were cultured as we described

previously (Nuttall et al., 2007). The tissues used were adjacent, but did not comprise, the epileptic focus in cortical areas. This material was used in accordance with the approval of the Research Ethics Board at the University of Calgary. In brief, the brain tissue targeted for excision was suctioned into a sterile bag retrieved with a Cavitron Ultrasonic Aspirator. The tissue fragments, of less than 2 mm^3 in size, were immersed within the sterile bag at room temperature (23 °C) by the saline that was used during surgery to keep the brain moist. Upon completion of the surgery, the sterile bag was transported within the hour at room temperature to the tissue culture laboratory for processing. In brief, the sterile bag content was transferred at room temperature into 50 ml tubes, removing the blood, meninges and clots by washing the tissue several times with PBS, and letting the brain tissue settle between washes. The content was transferred to a sterile 100 ml glass bottle for digestion with DNase (0.1 mg/ml) and 0.25% trypsin in PBS, and incubated at 37 °C for 25 min. Subsequently, FCS was added to inactivate the trypsin, and the sample was filtered through a sterile 130 μm mesh and centrifuged at 1200 rpm for 10 min. The sample was diluted in 21 ml of PBS and laid over 9 ml of Percoll in sterile 6–8 polycarbonate ultra-centrifuge tubes. The sample was mixed with a pipette and centrifuged at 15,000 rpm in a Beckman J2-21 M centrifuge with no brakes at 4 °C for 30 min. The myelin was then removed by aspiration from the upper layer, and the viable cell layer was recovered with a pipette and diluted 1:1 in PBS. The cells were washed twice in Complete MEM and recovered by centrifugation at 1200 rpm from 10 min (MEM + 0.2 mM Glutamine, 100 μg/ml Pen/Strep, 1X Non-essential amino acids, 1x Sodium pyruvate, 0.1% Dextrose and inactivated 10% FCS). Finally, the cells were suspended in medium, plated at 2×10^6 cells/ml in 5 ml uncoated T25 flasks and incubated for two nights at 37 °C in an atmosphere of 5% CO_2. The microglia adhered strongly to the flask, while the other cell types (principally oligodendrocyte precursor cells; neurons do not survive the isolation procedure while astrocytes are lost in the discarded Percoll fractions) remained in suspension or were only loosely attached. After removing the floating cells, the flasks were washed and trypsinized to obtain the microglia, which were then plated in poly-L-ornithine (0.01 mg/ml) coated 96-well plates at a density of 50,000 cells/100 μl medium. The cells were cultured for 3 days prior to treatment and then exposed to 2-AG (1 nM) for 24 h after 1 h of starvation in DMEM. Subsequently, pH Rodo particles were added to the culture media for 30 min and the cells were washed with live imaging buffer (Gibco). Calcein AM was then added to the medium and the cells were analyzed with a Molecular Devices ImageXpress high-content imaging system.

2.7. Rat microglia cultures

Primary microglia cell cultures from P0–P2 Wistar rats were prepared as described previously (Correa et al., 2009; McCarthy and De Vellis, 1980), with minor modifications (Mecha et al., in doi: https://doi.org//10.1038/protex.2011.218, Open Nature Exchange protocol only online). Purified microglia were plated at a density of 100,000 cells/cm^2 for PCR analysis, or at 50,000 cells/cm^2 for immunocytochemistry and phagocytosis assays. The cells were maintained for 3 days at 37 °C and in 5% CO_2, in a defined medium containing 10% horse serum and 10% FCS, and they were incubated for 1 h in serum-free DMEM prior to the pharmacological treatments. For RT-PCR studies, 2-AG (1 nM: Tocris Bioscience) was applied to the microglia cultures for 6 or 24 h. In another set of experiments, microglia were stimulated with 2-AG for 24 h and then purified myelin was added to the culture media for 6 h. In the case of the assay of myelin phagocytosis, 2-AG and TGF-β (20 ng/ml, PeproTech, Inc, UK) were applied for 24 h before the addition of the purified myelin.

2.8. In vitro myelin phagocytosis and immunocytochemistry

Rat microglial cells were grown on poly-D-lysine (5 μg/mL) coated glass coverslips and 1 h after serum starvation, they were exposed to 2-AG (1 nM), TGFβ (20 ng/mL) or both for 24 h. After this period, the microglia were washed with warm DMEM (37 °C) and exposed to 1 or 2 μg/mL purified myelin for 1 h. In a subset of experiments, myelin was labeled with Cy3 prior to its addition to the microglia cultures, as described previously. The cells were fixed with 4% PFA for 20 min and permeabilized with 0.1% Triton X-100 in PBS. After blocking with 5% normal goat serum (NGS), the microglial cells were incubated for 2 h at room temperature with a rabbit antiserum against mouse Iba-1 (1:500; 019-19741, WAKO) and MBP (1:500; MAB382, Millipore) in order to calculate the proportion of phagocytosing cells. After rinsing, glass coverslips were incubated for 1 h at room temperature with Alexa Fluor-conjugated antibodies (1:500, Molecular Probes, Inc), which were then mounted on slides with Mowiol and kept in the dark at 4 °C until they were analyzed on a laser scanning confocal microscope (Leica TCS-SP5). Myelin phagocytosis was evaluated *in vitro* and expressed as the percentage of phagocytic cells per field, the total amount of myelin phagocytosed within the cells and using an adaptation of the phagocytosis index described previously (see Natrajan et al. (2015)), which relates Cy3 fluorescence in the treated and control cells.

2.9. Immunoelectron microscopy and the g-Ratio

Mice were anesthetized deeply with pentobarbital (Doletal, 50 mg/kg body weight, i.p.), and perfused transcardially with 0.9% saline and then, with a fixative solution (2.5% PFA/2.5% glutaraldehyde). The brain of each mouse was then post-fixed in the same fixative solution for 40 min, washed with phosphate buffer (0.1 M), and sagittal vibratome sections were obtained from the corpus callosum (150 μm thick, Leica Microsystems). After washing the slices were incubated in osmium tetroxide (2% OsO_4 in 5.4% glucose/PB) for 1 h at room temperature, and dehydrated in an increasing acetone gradient. The samples were then embedded in Spurr's Resin (TAAB Lab Equipment Limited) and polymerization was achieved after incubation at 65 °C for 48 h. Ultrathin sections (65–70 nm) were obtained on an ultramicrotome (EM UC6; Leica, Graz, Austria), mounted on copper grids (200 mesh) and then examined with a transmission electron microscope (JEM-1200EX II: Jeol, Tokyo, Japan) operated at 80 kV. The images were recorded with a SIS Mega-View III CCD camera and the ImageJ software was used to evaluate the g-ratio of individual myelinated axons, a measure of myelin thickness as a function of the axon diameter. The g-ratio plug-in (http://gratio.efil.de) was employed on randomly selected axons in transverse sections of the corpus callosum using semi-thin light micrographs from each mouse analyzed. We performed measurements on a total of 100 selected axons per animal and the cumulative g-ratios were calculated for each mouse by averaging all the individual g-ratios.

2.10. Image processing and analysis

All confocal images were acquired on a Leica TCS SP5 confocal microscope. For *in vivo* studies, individual images of 4–5 sections of the corpus callosum (between bregma 1.10 mm to −1.06 coordinates) from at least 6 animals per group were analyzed. Immunostaining and cell counts were quantified using Fiji software (designed by the National Institutes of Health), evaluating the proportion of staining relative to the total area in Sham animals and the total number of cells/mm^2. In the case of microglia that internalized MBP, orthogonal views were captured in the z-direction in three different areas from the mouse corpus callosum using 40× objectives (with a 0.8 μm step size in the confocal stacks) and analyzed with Imaris. The total number of Iba-1^+ cells and the number of Iba-1^+ cells with internalized myelin (MBP staining inside the cell in the *in vivo* experiments or Cy3 staining inside the cell in the *in vitro* procedures) were counted using the cell counter plug-in of Image J. The MBP^+ area inside the Iba-1^+ cells was determined using the Image J co-localization plug-in, analyzing at least 20

microglial cells per section.

To determine the volume of MBP internalized by each microglial cell in the corpus callosum, a three-dimensional image from each microglia cell was created using the Imaris software. First, a surface corresponding to Iba-1 staining was created and then, to remove staining not at the microglia surface, a mask was created corresponding to the MBP channel setting all the voxels beyond that to 0. Finally, we created a second surface inside the microglial surface based on the mask of MBP positive staining exclusively within the cell. The "Number of voxels" filter was applied to each surface and the total volume of MBP inside the microglia, as well as total volume of each microglial cell was calculated for subsequent analysis. The volumes of MBP were quantified within at least 30 microglial cells.

For *in vitro* analysis, 2 μm step size confocal stacks were captured in the z-direction from 50 cells in 5 fields per experimental condition and experiment, using 20× objectives on the same confocal microscope (5 independent experiments were performed). Myelin phagocytosis *in vitro* was evaluated by determining the number of Iba-1$^+$ cells and the number of Iba-1$^+$ cells with internalized myelin (MBP$^+$) using the cell counter plug-in in Image J. These parameters were determined in 50 cells from 5 fields per experimental condition and experiment (5 independent experiments were performed). In vitro myelin uptake was determined after defining the single cell perimeter as the Cy3 area inside the selected area, measured as the average immunoreactivity in the red channel in the selected cell. The same threshold was set for all the cells and all experimental conditions.

2.11. Statistical analysis

Bar graphs represent the mean ± SEM and the data in scattered plots are expressed as the median ± range. GraphPad Prism software version 5.0 for Windows and SPSS 22 software (IBM Corporation, USA) were used for the statistical analysis. The normality of the data was assessed with a Barlett's test. The p values were obtained with a Student's two tailed *t*-test and one-way analysis of variance (ANOVA) was used for multiple comparisons, followed by a Bonferroni post-hoc test to determine the statistical significance. Whenever normality was not achieved, statistical significance was determined with non-parametric tests (Kruskal-Wallis and post-hoc pair-wise comparisons with a Mann-Whitney *U* test). Benjamini-Hochberg's correction was applied to control multiple testing in the *in vivo* RT-PCR data analysis, setting the significance threshold to 3% as adjusted P value. The analysis of covariance was used to analyze regression lines. The level of significance was set at $^*p$ adjusted $\leqslant 0.03$ for *in vivo* RT-PCR analysis, and $^*p \leqslant 0.05$ for the others; $^{**}p \leqslant 0.01$; and $^{***}p \leqslant 0.001$.

3. Results

3.1. Corpus callosum demyelination mobilizes OPCs and microglia along with reduced synthesis and degradation machinery of eCBs

From a therapeutic point of view, demyelination in the TMEV-IDD mouse MS model has commonly been studied in the spinal cord and related to the motor deficits evident in these mice (Feliú et al., 2017). Yet in the preclinical stage, demyelination can also be observed in non-classical demyelinated structures like the brainstem, cerebral cortex (Mecha et al., 2013a) and even, the corpus callosum (Mecha et al., 2013b). Significantly, this demyelination is followed by a spontaneous and incomplete process of remyelination that declines in the chronic phase of the disease. Here, we have focused on the corpus callosum as one of the major white matter structures in the brain. Immunohistochemical analysis of MBP staining showed that demyelination was extensive 35 days after TMEV intracerebral infection, with a loss of 95% of the area occupied by MBP compared to Sham mice (Fig. 1a, b). This loss of MBP was accompanied by a significant decrease in *mbp* and *plp* mRNA, the two major myelin proteins in the CNS (Fig. 1c). This marked demyelination was not associated with the loss of mature oligodendrocytes, as no change in the number of CC1$^+$ oligodendrocytes was observed (Fig. 1d, e). Remarkably, more OPCs (Olig-2$^+$/CC1$^-$) were found in the corpus callosum, which was probably related to the mobilization and fast differentiation of OPCs into pre-myelinating oligodendrocytes, as suggested by the diminished *olig-2* gene expression (Fig. 1f).

The inflammatory milieu is a mediator of remyelination (Franklin and Ffrench-Constant, 2008) and in the demyelinated corpus callosum, while there were more Iba-1$^+$ microglial cells, no change in the area occupied by these cells was evident by immunohistochemistry (Fig. 1g, h). When we analyzed the mRNA expression of inflammatory mediators and chemokine genes, we found that demyelination did not alter the expression of the pro-inflammatory cytokines *tnf-α* or *il-1*β, whereas the expression of the anti-inflammatory cytokine *il-10* (Fig. 1i) and that of the chemokine *ccl-2* increased. Conversely, there was a significant downregulation of *cxcl-12*, *sema3A* and *sema3F* expression (Fig. 1j). As the eCB system is thought to be dysregulated in MS and in the EAE murine model (Centonze et al., 2007), we studied the 2-AG and AEA synthetic and degradation machinery in the corpus callosum by RT-PCR. Surprisingly, the 2-AG and AEA synthesis and degradation machinery was dampened in this demyelinated structure (Fig. 1k), with reduced expression of the main enzyme responsible for the synthesis of 2-AG (*dagl-α* diacylglycerol lipase-*α*) while the reduction in its hydrolysis enzyme did not reach statistical significance (*magl*-monoacylglycerol lipase). The enzymes that account for the synthesis (*nape-pld*) and degradation (*faah*) of AEA were both reduced. By contrast, the expression of these enzymes did not change in the adjacent cerebral cortex (Fig. S1), suggesting a specific reduction in the synthesis enzymes of the two major eCBs in demyelinated white matter lesions.

3.2. 2-AG modifies microglia activation state in demyelinated corpus callosum

Taking into account the reduced eCB synthesis machinery in the demyelinated corpus callosum and to evaluate the potential influence of eCBs on spontaneous remyelination, we administered 2-AG to TMEV infected mice using subcutaneous mini-osmotic pumps that were implanted on day 28 pi to mediate its constant delivery. On day 35 pi, 7 days of 2-AG delivery did not modify the loss of MBP in the corpus callosum (Fig. 2a), or the downregulation of *mbp*, *plp* and *olig-2* gene expression relative to the vehicle-treated TMEV mice (Fig. 2b). Accordingly, the number of mature oligodendrocytes and OPCs in the demyelinated corpus callosum did not differ between the two experimental groups (Fig. 2c), although there were fewer OPCs in the adjacent cortex in the animals that had been treated with the eCB (Fig. S2). Remarkably, the immunostaining for Iba-1 was enhanced in the mice administered 2-AG (Fig. 2d). While there was no difference in the number of Iba-1$^+$ microglia in the demyelinated corpus callosum of 2-AG and vehicle-treated TMEV mice, the area occupied by these cells was significantly larger in the animals that received 2-AG (Fig. 2e), probably due to the activation of microglia in the demyelinated corpus callosum that was not significant in the adjacent cortex (Fig. S2). The significant increase in the expression of the inflammatory markers *tnf-α* and *il-1*β further suggested the activation of microglia in mice administered 2-AG, although we also observed higher levels of *il-10* (Fig. 2f). Moreover, we found an upregulation in the expression of *cxcl-12* and *sema3F* mRNA relative to the vehicle-treated mice (Fig. 2g, h). In terms of the eCB machinery, RT-PCR analysis showed enhanced AEA synthesis enzyme (*nape-pld*) with a tendency to increase *faah* expression, and no alteration to 2-AG synthesis or degradation enzymes (Fig. 2i). No differences were found when the expression of inflammatory mediators and enzymes related to eCB machinery was analyzed in the adjacent cortex relative to TMEV-Vehicle mice (Fig. S2). Our results suggest that exogenous administration of 2-AG partially restores the eCB enzymes machinery expression in the demyelinated

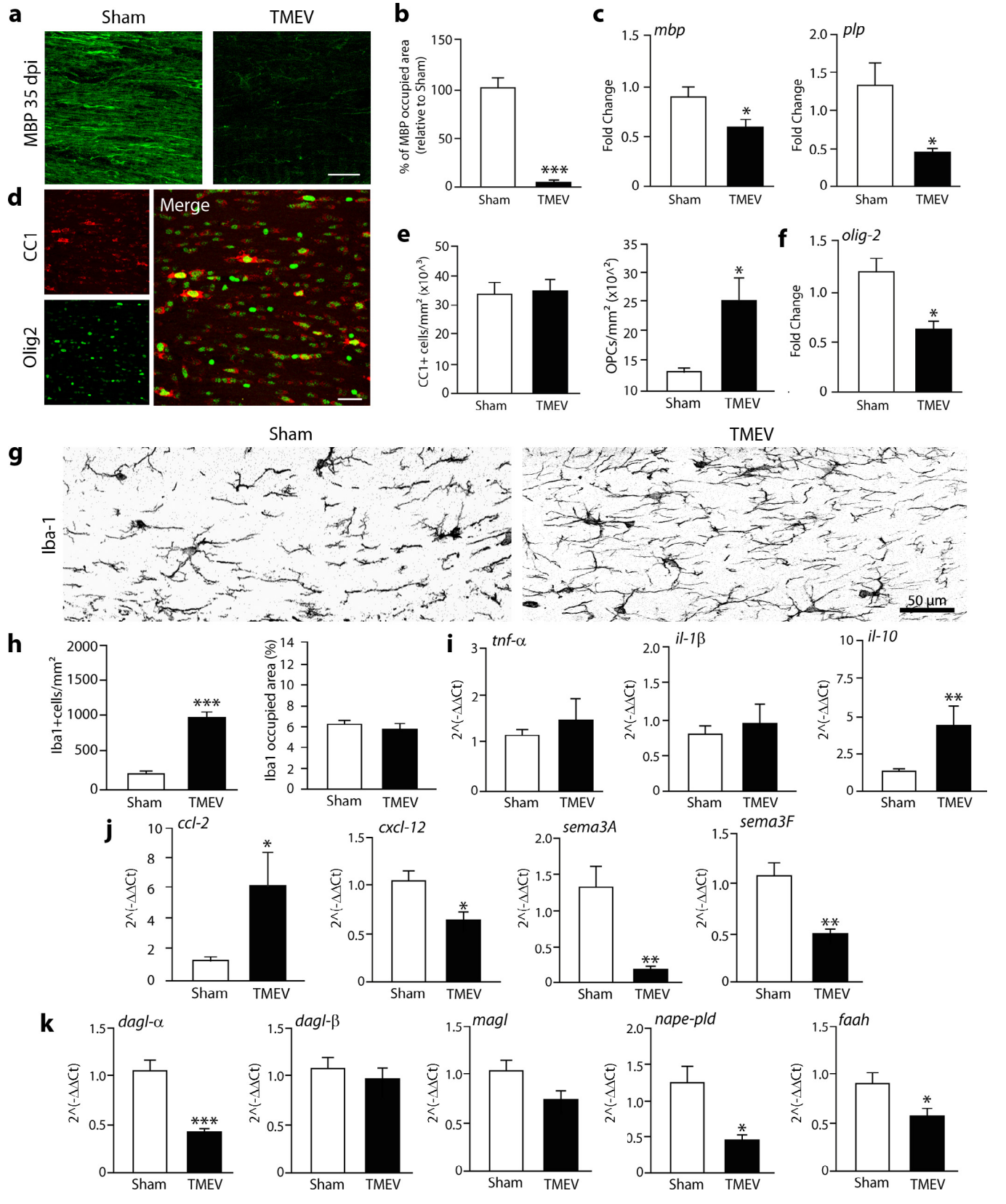

(caption on next page)

corpus callosum, and it also elicits the activation of microglial cells that could affect the ensuing remyelination.

At 42 dpi, a considerable increase in MBP staining was evident in the corpus callosum of TMEV mice (Fig. 3a) relative to day 35 pi, indicating the initiation of endogenous repair. When the area occupied by MBP was analyzed, there was a significant increase in TMEV mice relative to 35 dpi, that was further enhanced following the administration of 2-AG over the previous 14 days (Fig. 3b). The remyelination

Fig. 1. Corpus callosum demyelination mobilizes OPCs and microglia along with reduced synthesis and degradation machinery of eCBs at 35 dpi. (a) MBP immunofluorescence to measure the myelin content in the corpus callosum (CC) at 35 dpi, (b) data quantification shows a prominent loss in MBP content in TMEV infected mice; (c) RT-PCR analysis of MBP and PLP mRNAs shows a significant reduction in the myelin protein synthetic machinery. (d) Olig-2/CC1 dual immunofluorescence in the CC discriminates mature oligodendrocytes ($Olig2^+CC1^+$) and OPCs ($Olig2^+CC1^-$). (e) The quantification of dual immunofluorescence highlights the increase in OPC number in TMEV mice, accompanied by a decrease in Olig-2 expression evident by RT-PCR (f). (g, h) Iba-1 staining in the demyelinated CC shows no apparent changes in the activation of microglia with an increase in the number of these cells (h). The inflammatory milieu in the CC was analyzed by RT-PCR, assessing the cytokines, *tnf-α*, *il-1*β and *il-10* (i) the chemokines, *ccl-2* and *cxcl12* and the semaphorins, *sema3A* and *sema3F* (j). (k) Quantification of the expression of enzymes involved in the synthesis and degradation of 2-AG and AEA showing reduced *dagl-α*, *nape-pld and faah* gene expression following demyelination. Each point represents the mean ± SEM from 5 to 7 mice per group: *p adjusted ≤ 0.03; **p ≤ 0.01; ***p ≤ 0.001 *vs*. Sham mice. Scale bar: 25 μm (a, d) and 50 μm (g).

that underlies the increased MBP staining was accompanied by an increase in the number of OPCs relative to 35 dpi (Figs. 3c and 2c). Indeed, there was also a significant increase in the number of OPCs in the adjacent cortex (Fig. S3). At this time, the morphological changes related to activation of microglial cells in the corpus callosum were prominent in vehicle and 2-AG treated mice (Fig. 3d), together with a significant increase in the area occupied by Iba-1, without affecting the total number of microglial cells relative to 35 dpi (Figs. 3e and 2e). This increase in the area occupied by microglia at 42 dpi was also found in the cerebral cortex, where 2-AG treatment diminished the reactivity of these cells without modifying the increase in their number (Fig. S3). The expression of the *tnf-α* gene was upregulated in both experimental groups, whereas *il-1*β was only enhanced in the mice that received vehicle and *il-10* expression shows a tendency to increase in 2-AG

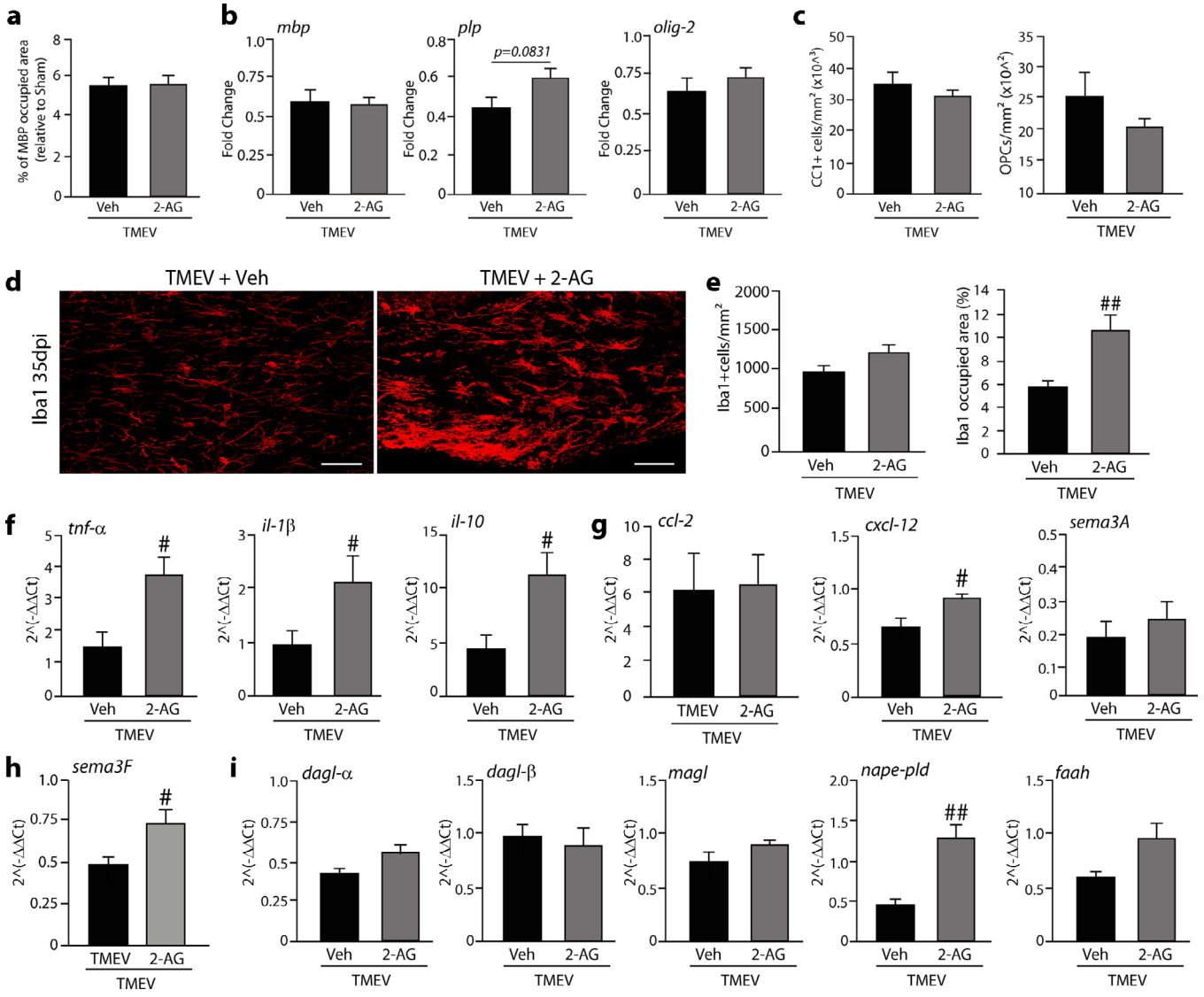

Fig. 2. 2-AG administration modifies microglia activation state in demyelinated corpus callosum at 35 dpi. No differences are found between 2-AG and Vehicle treated TMEV mice in: (a) the proportion of MBP quantified by immunohistochemistry, (b) *mbp*, *plp* or *Olig-2* mRNA analyzed by RT-PCR, or the number of mature oligodendrocytes and OPCs (c). 2-AG treatment increases the Iba-1 staining in the CC evident by immunohistochemistry (d), showing an increase in the area occupied by microglia with no change in the total number of microglial cells (e). RT-PCR analysis shows that 2-AG increases the levels of the cytokines *tnf-α*, *IL-1*β *and IL-10* (f) and the chemokine *cxcl-12* (g) and *sema3F* (h) mRNAs, restoring the expression of the machinery involved in the synthesis of AEA without affecting the 2-AG metabolic enzymes (i). Each data point represents the mean ± SEM from 5 to 7 mice per group: $^{\#}$p adjusted ≤ 0.03; $^{\#\#}$p ≤ 0.01 *vs*. TMEV + Veh. Scale bar: 50 μm.

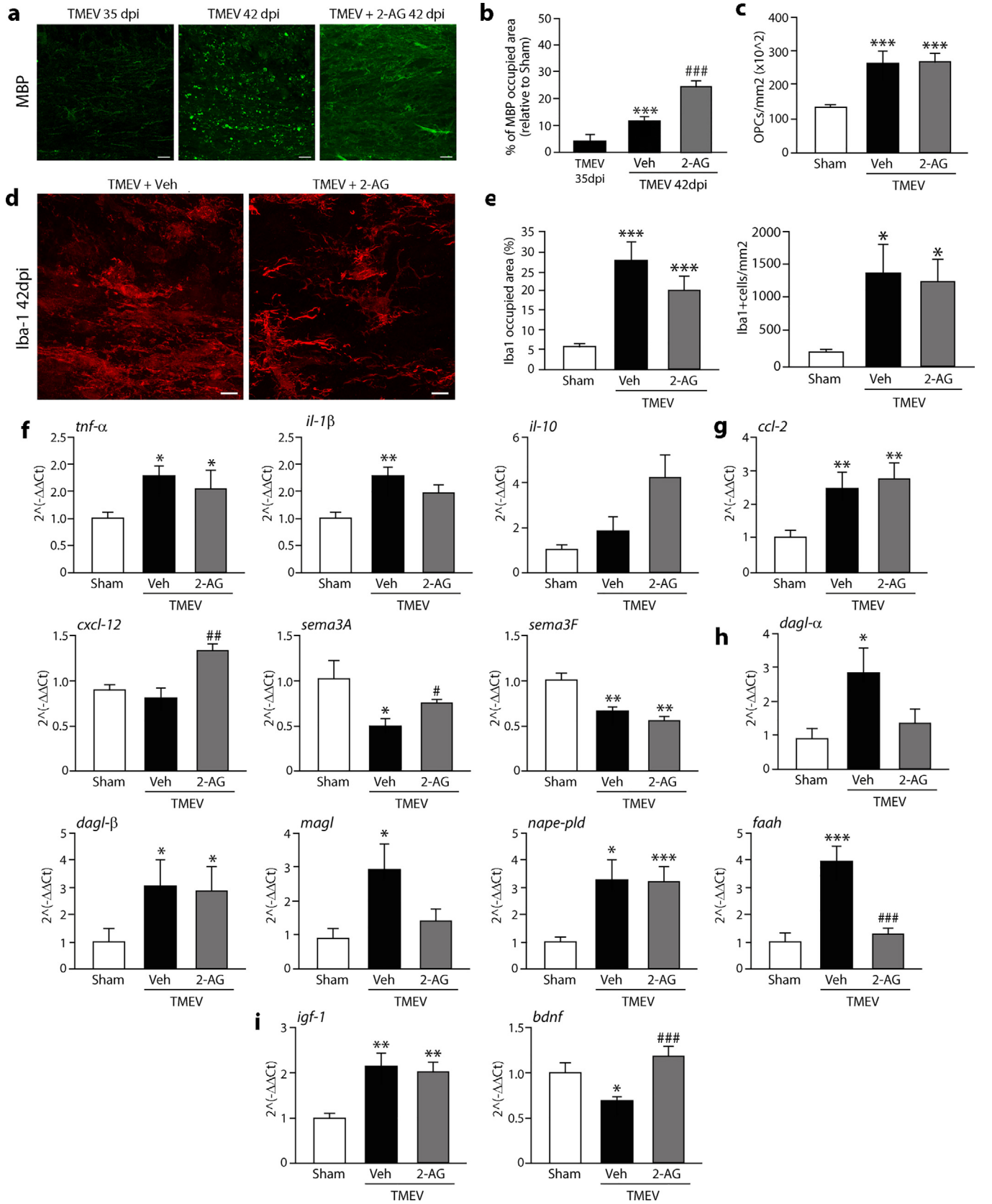

Fig. 3. 2-AG promotes endogenous remyelination at 42 dpi. Remyelination is evident in the CC at 42 dpi, as witnessed by MBP immunostaining when comparing TMEV infected mice at 42 and 35 dpi (a). 2-AG further promotes the increase in the area occupied by MBP (b), without affecting the total number of OPCs (c). Microglial activation at 42 dpi is highlighted by Iba-1 immunofluorescence (d), although no changes are found in the area occupied by microglia or in the total number of cells by 2-AG (e). RT-PCR studies of the corpus callosum analyze the expression of the cytokines *tnf-α*, *IL-1β and IL-10* (f), the chemokines, *ccl-2* and *cxcl12* and the semaphorins, *sema3A* and *sema3F* (g), enzymes involved in the synthesis and degradation of eCBs (h), and the growth factors *igf-1 and bdnf* (i). Each point represents the mean ± SEM from 6 to 10 mice per group: *p adjusted ≤0.03; **p ≤ 0.01; ***p ≤ 0.001 *vs.* Sham; $^{\#\#}$p ≤ 0.01; $^{\#\#\#}$p ≤ 0.001 *vs.* TMEV + Veh. Scale bar: 25 μm (a), 10 μm (b).

treated mice (Fig. 3f). This profile was confined to the remyelinating corpus callosum, since no significant changes were found in the adjacent cortex (Fig. S4). Immunohistochemistry and RT-PCR for *nos-II* and *arg-1* in the corpus callosum was performed to further analyze the inflammatory profile of microglia, yet no differences were found between the two experimental groups (Fig. S5).

Chemokine expression was affected by eCB treatment, with enhanced *ccl-2* mRNA and reduced levels of *sema3F* in both groups (42 dpi, TMEV + vehicle and TMEV + 2-AG), while *cxcl-12* was enhanced and *sema3A* partially restored in 2-AG treated mice (Fig. 3g). Regarding eCB biosynthesis and inactivating machinery, RT-PCR analysis showed a general increase in the expression of the main synthesis enzymes of 2-AG or AEA in both groups, whereas the hydrolysis enzymes were only upregulated in TMEV mice that received vehicle (Fig. 3h), perhaps related to the endogenous process of remyelination. In the adjacent cortex, non-significant changes were observed in eCB metabolic machinery expression following 2-AG treatment (Fig. S4). In the corpus callosum (Fig. 3h), exogenous 2-AG administration did not modify *dagl-α* or *magl* levels compared to the Sham mice, whereas *dagl-β* was increased and the AEA synthesis enzyme *nape-pld* was upregulated without affecting the degradation enzyme *faah*. These changes were probably due to adjustments in the eCB system related to the continuous release of 2-AG by the miniosmotic pumps. The aforementioned changes were found in conjunction with increased expression of *igf-1* involved in CNS remyelination and repair, both in vehicle and 2-AG treated mice, while exogenous 2-AG restored the expression of the *bdnf* gene that was downregulated in vehicle-treated TMEV mice (Fig. 3i).

3.3. 2-AG boosts myelin debris phagocytosis

Myelin debris has been related to the inhibition of OPC differentiation, impairing remyelination (Kotter et al., 2006). Given the changes in microglial activation associated with demyelination in the corpus callosum, we further studied the possible implication of these cells in the phagocytosis of myelin debris. The expression of genes associated with myelin phagocytosis and the overall phagocytic machinery was analyzed by RT-PCR. One of the mechanisms by which myelin downregulates its own phagocytosis is through the expression of CD47 by myelin, and SIRP*α* by microglia and macrophages (Gitik et al., 2011). In our experimental model of demyelination, this interaction was diminished significantly on day 35 pi compared to Sham mice (Fig. 4a), suggesting a potential deficit in the phagocytosis of myelin debris by microglia and/or macrophages. However, no changes were found when we compared *sirpα/cd47* expression in mice administered with the vehicle alone or with 2-AG. In terms of the expression of other phagocytosis associated genes, we evaluated those implicated in the general phagocytic machinery (*cd206*, *msr1*, *cd68* and *mgf-e8*: Fig. 4b) and in phagosome assembly (*lamp1* and *lamp2*: Fig. 4c). These molecules are upregulated *in vitro*, in conjunction with an enhanced capacity of microglia to phagocytose myelin following IFNβ stimulation (Kocur et al., 2015). In TMEV mice, we observed a tendency to downregulate *cd206* and a significant reduction of *mgf-e8* mRNA expression compared to the Sham mice, whereas 2-AG administration increased *msr1* expression at 35 dpi. By contrast, there were no significant changes on the expression of *cd68*, *lapm1* or *lamp2*. At 42 dpi *sirpα/cd47* gene expression was restored to Sham levels in both experimental groups (Fig. 4d). The expression of some of the genes involved in the general phagocytic machinery was upregulated in the mice that received the vehicle alone, *cd206*, *cd68* and *mgf.e8*, although increased *msr1* expression did not achieve statistical significance (Fig. 4e). In the case of the genes associated with phagosome assembly, 2-AG treatment enhanced the expression of *lamp-1* in comparison to the Sham mice (Fig. 4f). Although our study is limited by the lack of proteins measurement, we underline the increased gene expression of *msr1* and *lamp1* by 2-AG.

To assess specifically the phagocytosis of myelin debris by microglia, we performed dual immunohistochemistry of MBP and Iba-1 in the corpus callosum, focusing on MBP profiles within microglia at 35 and 42 dpi highlighted in the orthogonal views of confocal stacks (Fig. 5a, c). These confocal projections were used to study the proportion of microglia with internalized MBP, which indicated that there were no changes between the two experimental groups on day 35 pi (Fig. 5a, b). Nevertheless, 2-AG administration boosted microglial myelin phagocytosis to 100% of the cells by 42 dpi (Fig. 5c, d). Finally, MBP phagocytosis by microglia was studied using Imaris software (Fig. 5e), which showed a significant decrease in the amount of MBP internalized by microglia in TMEV mice at 42 dpi compared to 35 dpi (Fig. 5f, g). Interestingly, 2-AG administration enhanced the amount of MBP phagocytosed by microglia at 42 dpi (Fig. 5f, g: see the online Videos of the 3D microglial surfaces with internalized MBP in TMEV-Veh and TMEV-2-AG: Supplementary V1 and V2, respectively).

In an attempt to show the direct effects of 2-AG on microglial phagocytosis, we used *in vitro* functional approaches with human and rat microglial cells. *E. Coli*-coated beads were employed to measure the phagocytic capacity of human microglia in the presence or absence of 2-AG (Fig. 6a). Exposure to 2-AG (1 nM, 24 h) significantly enhanced phagocytosis by human microglial cells (Fig. 6b). We then studied the effects of 2-AG on the expression of phagocytosis associated genes by microglia obtained from post-natal rat brains. When 2-AG (1 nM) was added to the culture media for 6 h, there was a significant increase in *cd206*, *msr1*, *sirp1α* and *trem2* mRNA compared to control microglia, without affecting the expression of *scarb1*, *lamp1* and *lamp2* (Fig. 6c). These effects were temporary and 24 h after 2-AG exposure, only *trem2* remained significantly upregulated (Fig. 6d). To approximate our *in vitro* results to those obtained in our model of demyelination we purified myelin from the adult rat brain and added it to microglia cultures to assess whether 2-AG treated microglia (1 nM, 24 h) also improved the expression of phagocytosis associated genes in the presence of myelin, as well as to assess myelin phagocytosis itself. RT-PCR analysis showed that when myelin was present in the culture medium for 6 h, the *cd206*, *msr1* and *lamp1* gene expression augmented in 2-AG-treated microglia relative to vehicle treated cells (Fig. 6e). Indeed, 2-AG pretreatment for 24 h improved the proportion of microglia that phagocytosed MBP^+ myelin over 1 h, achieving the same effect as the pro-phagocytic factor, TGF-β. Nevertheless, no additive effects were found when 2-AG and TGF-β were added together (Fig. 6f). In fact, the maximal level of microglial phagocytosis was reached 2 h after myelin addition to the culture media. Given that the phagocytic index of microglia stimulated with 2-AG was the same as that seen after stimulation with TGF-β (Fig. 6g), we analyzed the Cy3-labeled myelin internalized by microglia after 1 h when cells were pre-treated with 2-AG for 24 h in the presence of selective antagonists of CB1 and CB2 receptors. A significant increase in the area of myelin internalized by microglia was elicited by 2-AG exposure, with the involvement of both CB1 and CB2 receptors in this pro-phagocytic response (Fig. 6h, i). Previously, we had found that microglia derived from $CB2^{-/-}$ deficient mice diminished their phagocytic capacity (Mecha et al., 2015).

3.4. 2-AG restores the myelin content and myelin sheath thickness

Consistent with our earlier observations, the demyelinated corpus callosum of TMEV mice shows a prominent increase in the labeling of the myelin markers, MBP and PLP at 60 dpi (Fig. 7a, c). Although this increase reaches 60% of the myelin content of Sham mice, it is enhanced notably, to 100%, when TMEV mice were administered 2-AG from 28 to 42 dpi, stressing the positive effects of this eCB in the remyelination process (Fig. 7b, d). Indeed, there was a strong relationship between the increase in MBP or PLP staining and the increased myelin sheath thickness at the ultrastructural level in mice that received 2-AG (Fig. 7e). When analyzing the g-Ratio (the ratio of axon diameter to the outer diameter of the myelin sheath), we found that it was lower in mice administered 2-AG than in those that received the vehicle alone.

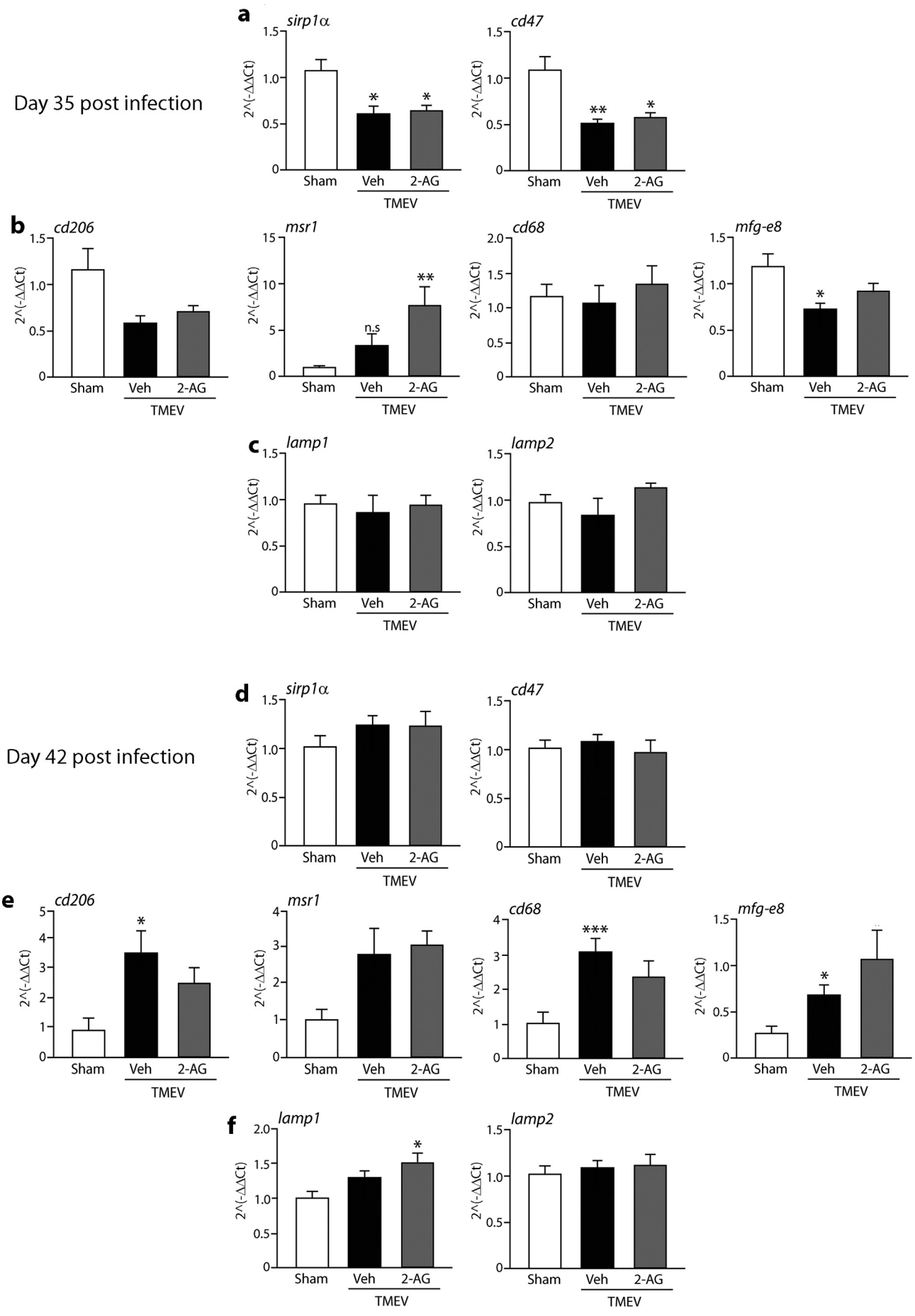

(caption on next page)

Fig. 4. Expression of phagocytosis associated genes at 35 and 42 dpi in the CC. RT-PCR at 35 and 42 dpi to study the expression of the myelin phagocytosis genes *sirp1α* and *cd47* (a, d), molecules functionally involved in the general phagocytic machinery (b, e) and lysosome-associated membrane proteins involved in phagosome assembly (c, f). Each point represents the mean ± SEM from 10 mice per group: *p adjusted ≤0.03; **p ≤ 0.01; ***p ≤ 0.001 *vs.* Sham mice.

Hence, a thicker myelin sheath formed around the small caliber axons analyzed (Fig. 7f, g). The reparative effects of 2-AG were also evident in the total number of mature oligodendrocytes and progenitors, which were both significantly higher in the animals that received the eCB (Fig. 7h). Finally, the number of microglia and their reactivity was significantly higher in TMEV mice, whereas both these parameters were dampened in mice administered 2-AG, reaching the levels in Sham mice (Fig. 7i). This phenomenon was probably related to the restoration of homeostasis subsequent to complete remyelination.

4. Discussion

Understanding the mechanisms that orchestrate remyelination is essential to develop effective therapeutic strategies in MS. Besides the presence of functional intact axons, successful remyelination requires the timely migration of OPCs into the demyelinated lesion (Harlow et al., 2015), inflammation-dependent OPC activation to drive their differentiation into myelinating oligodendrocytes (Miron et al., 2011), and the effective removal of myelin debris by phagocytes (Baer et al., 2009). Therefore, it has been hypothesized that the failure to undergo remyelination in MS might be due to a temporal discordance between OPC migration into the lesion, and the inflammation required for OPC activation and differentiation provoked by myelin breakdown (Miron et al., 2011). In the present study, we used the TMEV-IDD viral model of MS to analyze the dynamics of remyelination in the corpus callosum. In the preclinical phase of this model, there was prominent demyelination in the corpus callosum 35 days after TMEV infection, which was followed by spontaneous remyelination evident at 60 dpi (Mecha et al., 2013b). Compared to uninfected mice, the dynamics of demyelination/remyelination in TMEV animals constituted 5% of the total MBP staining in the corpus callosum at 35 dpi, increasing to 12% of the area occupied by MBP staining at 42 dpi, and finally, to 60% of the MBP and PLP immunostaining by 60 dpi. We therefore focused on these three time points – 35, 42 and 60 dpi – to study the mechanisms underlying corpus callosum remyelination in the TMEV-IDD model.

First, we found that corpus callosum demyelination at 35 dpi was accompanied by a decrease in MBP and PLP gene expression but not by a loss of mature oligodendrocytes. Nevertheless, the number of OPCs increased in the corpus callosum at this time, together with reduced Olig-2 expression that is presumably due to OPC maturation (Mei et al., 2013). To rule out the possibility of OPC recruitment from nearby regions, we analyzed the number of progenitors in the adjacent cerebral cortex and no differences were found between TMEV and Sham mice, suggesting that the demyelinated area is repopulated by OPCs derived from local, proliferating OPCs. However, we previously failed to find more proliferating $NG2^{+}$ OPCs at 35 dpi or changes in their morphology (Mecha et al., 2013a). Thus, it is likely that the acute inflammation that provokes demyelination in the corpus callosum following TMEV infection provides the local stimulus for OPC proliferation in the early stages of the model. Furthermore, and since activation of the subventricular zone has been found at this time (Mecha et al., 2013a), the contribution of subventricular progenitors to remyelination in the corpus callosum still needs to be clarified.

Oligodendrocyte recruitment and differentiation is regulated by numerous environmental factors, including cytokines, chemokines, semaphorins and growth factors among others (Plemel et al., 2017). In particular, the balance between Sema3A (chemorepellent for OPCs) and Sema3F (an attractive migratory cue for OPCs) is one of the elements that seems to be dysregulated in MS lesions, with increased Sema3A expression apparently blocking OPC recruitment (Boyd et al., 2013). Here, we found that both chemoattractant and chemorepellent cues were downregulated at the mRNA level in the demyelinated corpus callosum at 35 dpi, together with reduced *cxcl-12* gene expression, a potent chemoattractant implicated in OPC recruitment for remyelination (Patel and Klein, 2011).

In terms of microglia, we found more microglial cells in the corpus callosum and adjacent cortex at 35 dpi, with no apparent changes in their reactivity. Microglial cells are considered among the most versatile cells owing to their capacity to adapt to their ever changing microenvironment. Microglia produce and respond to anti-inflammatory cytokines like IL-10, inducing neuroprotective (Streit et al., 2005; Hanisch and Kettenmann, 2007) and oligoprotective effects (Molina-Holgado et al., 2001). Indeed, IL-10 has been implicated in the induction of an acquired-deactivation state related to debris scavenging, and in the pro-healing activity of microglia. The selective increase in *il-10* gene expression in the demyelinated corpus callosum of TMEV mice might be associated to the homeostatic responses to damage that are designed to: i) maintain microglia in a deactivated state and avoid the deleterious effects of excessive inflammation; and ii) promote repair by protecting the repopulating OPCs from damage.

The expression of genes responsible for the synthesis and degradation of the two main eCBs is weaker in the demyelinated corpus callosum at 35 dpi, although the increase in MBP immunostaining suggests this mRNA expression recovers at 42 dpi when the process of remyelination appears to have started in TMEV-IDD. In the cuprizone model of demyelination elevated transcripts and protein levels of hydrolysis enzymes of 2-AG, MAGL, ABHD6 and ABHD12 have been observed in corpus callosum without changes in 2-AG levels (Manterola et al., 2018). In this respect, many discrepancies have been reported on the levels of eCBs in the EAE model of MS when the immunized animals were rats or mice. In rats, 2-AG and AEA were found to be diminished in several areas of the CNS in acute EAE whereas mice showed increased synthesis and decreased degradation provoking elevated levels of AEA in the brains of EAE mice in the acute phase of the disease (Centonze et al., 2007); this last work also found increased AEA levels in the CSF of relapsing MS patients. Though positive and negative changes in eCBs levels have been reported to occur in the same pathological condition with both protective and worsening effects (Di Marzo et al., 2004; Pacher et al., 2006), cumulative evidence sustains the view of the efficacy of eCB signaling to control neuroinflammation (Walter and Stella, 2004). Even though we did not measure the levels of 2-AG and AEA in the corpus callosum, the reduced gene expression of the machinery implicated in the synthesis and degradation of eCBs may be presumptive of an overall reduction in their bioavailable levels at day 35 pi, whereas at day 42 pi the recovered metabolic eCBs enzymes suggest re-established levels of these bioactive lipids likely associated with their homeostatic and reparative roles. As such, it seems rational to administer 2-AG before day 35 in order to investigate how exogenous 2-AG may influence endogenous remyelination. Although 2-AG administration did not alter markers of myelin, or the number of mature oligodendrocytes, OPCs or microglia countings in the corpus callosum at 35 dpi, it was observed stronger microglial immunoreactivity. Even in absence of proteins measurement, the RT-PCR data with upregulated *tnf-α* and *il-1β*, in conjunction with increased *il-10* suggest augmented inflammatory mediators as a result of microglia activation. Given that TMEV mice show a spontaneous activation of microglia at 42 dpi, likely related to the uncoupling of inflammation after the onset of remyelination, we think that 2-AG prompts a moderate inflammatory response at 35 dpi in the damaged corpus callosum but not in adjacent cortical areas. In the acute phase of TMEV-IDD model, pro-inflammatory cytokine genes are upregulated 100 times compared to uninfected Sham mice (Mecha et al., 2018). Taking into account this

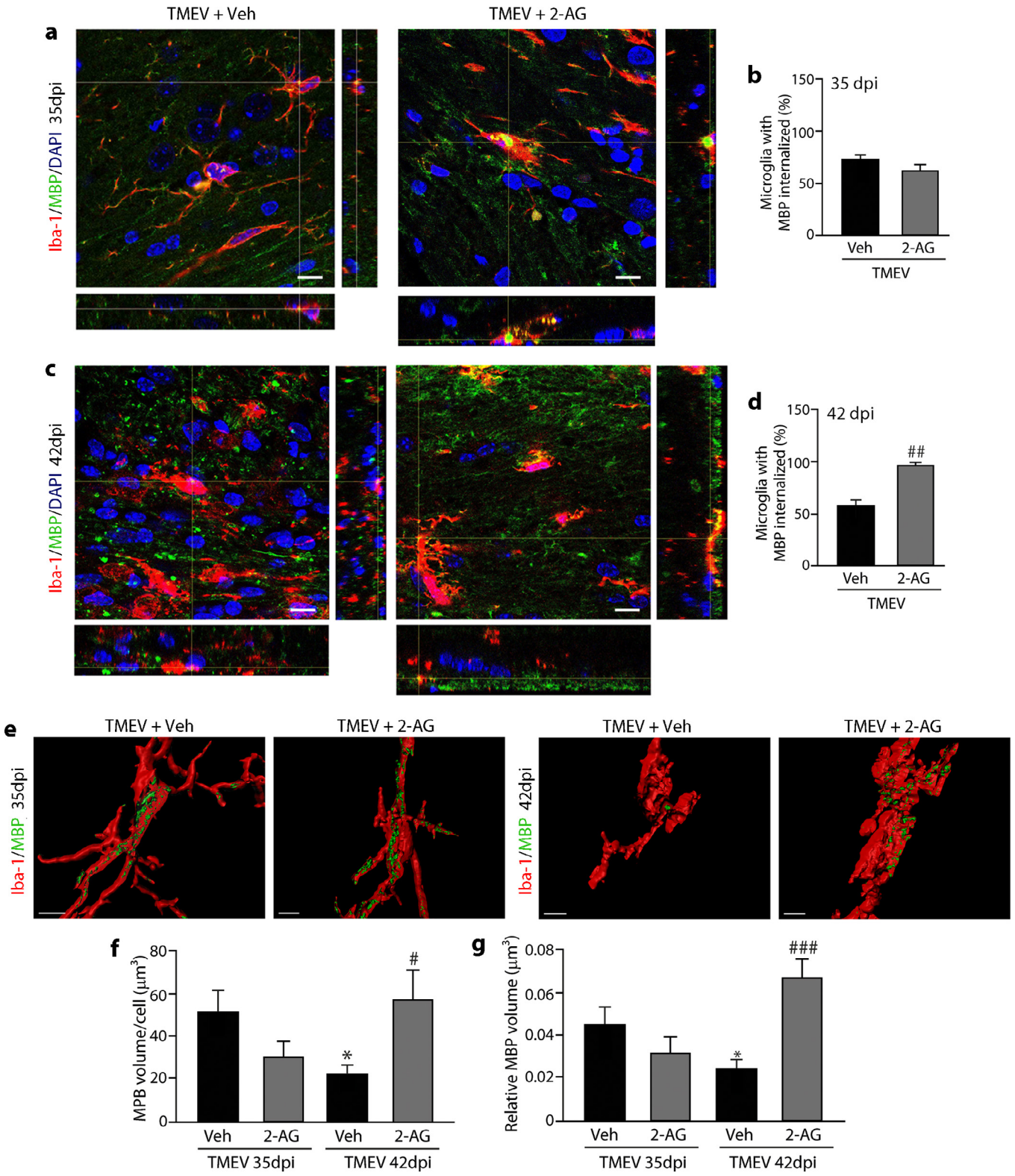

Fig. 5. 2-AG improves myelin debris clearance by microglia following demyelination in the corpus callosum. Orthogonal views of triple Iba-1/MBP/DAPI immunofluorescence at 35 (a) and 42 (c) dpi in the corpus callosum, revealing myelin phagocytosis by microglia. The proportion of microglia with internalized MBP was quantified in confocal projections of the immunofluorescence images. No differences can be found between the two experimental groups at 35 dpi (b); yet 2-AG treatment improves the proportion of these phagocytic cells to 100% at 42 dpi (d). Imaris software was used to analyze the volume of the MBP inside the microglia, and representative snapshots of the surfaces created for both Iba-1 and MBP are shown (e). Quantification of the total volume of MBP per microglia cell (f), as well as the volume of MBP relative to the volume of microglia (g), shows that MBP internalization in Vehicle-treated mice decreases at 42 dpi but it improves in those animals that were treated with 2-AG. Each point represents the mean ± SEM from 3 mice per group: $^{*}p \leq 0.05$ *vs.* Sham mice; $^{\#}p \leq 0.05$, $^{\#\#}p \leq 0.01$; $^{\#\#\#}p \leq 0.001$ *vs.* TMEV + Veh. Scale bar: 10 µm (a c) and 5 µm (e).

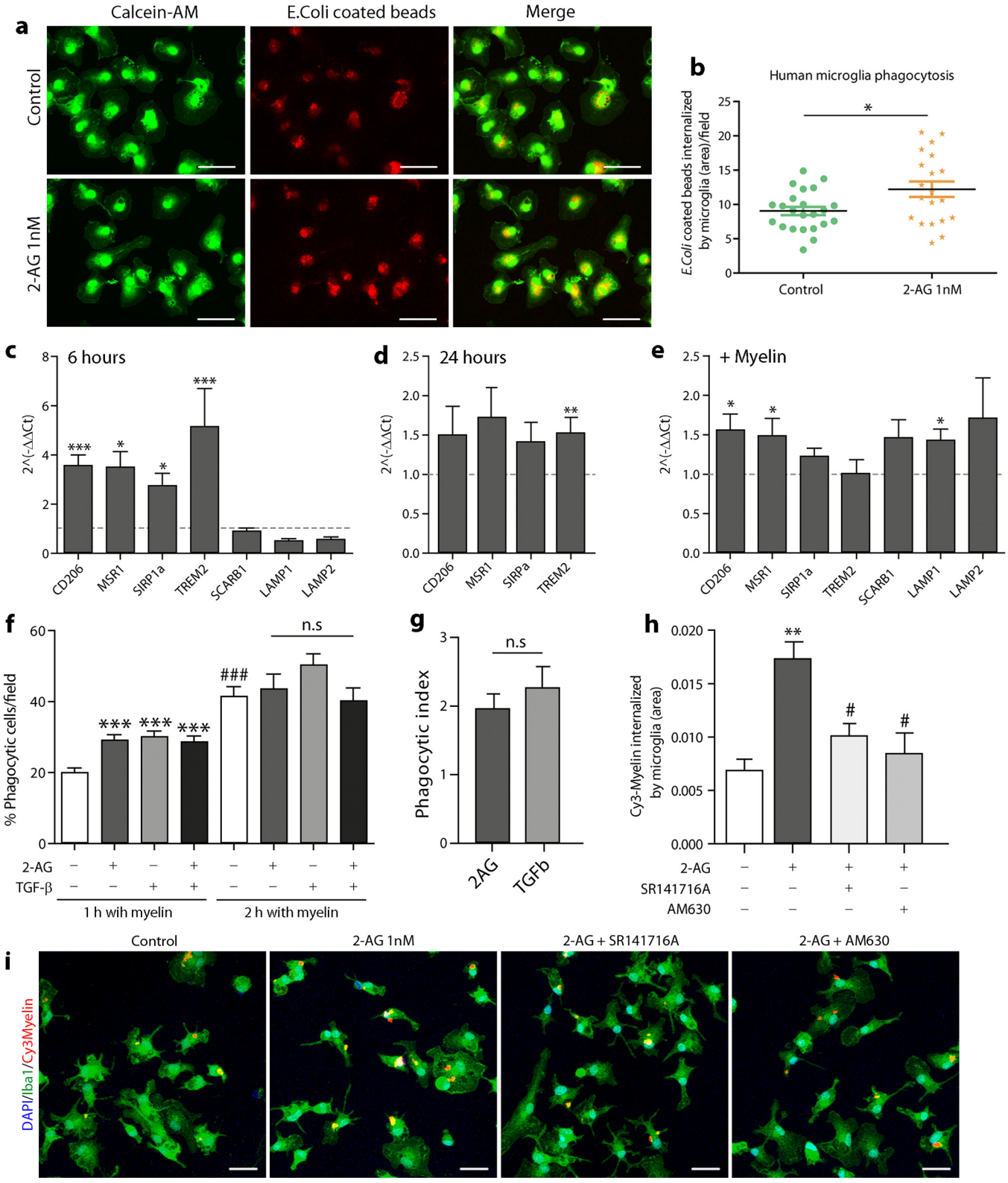

(caption on next page)

strong increment in pro-inflammatory mRNA levels in response to the viral infection, we take on that the 2–4 fold up-regulation of *tnf-α*, *il-1*β and *il-10* that we have found here suggests a mild inflammation. Indeed, the spontaneous remyelination that ensued in the corpus callosum of vehicle-TMEV animals did not reach the levels seen in Sham mice, with only partial immunostaining of the myelin proteins MBP and PLP, and a higher than normal g-Ratio in the adult corpus callosum (estimated to average 0.75: Bercury et al., 2014). Notably, the myelin immunostaining in 2-AG- treated TMEV mice coupled to the lower g-Ratio at 60 dpi suggests that administering this eCB engages inflammation to OPC differentiation, and that, 2-AG thereby enhances spontaneous remyelination. The number of mature oligodendrocytes

Fig. 6. 2-AG boosts microglial phagocytosis *in vitro*. A non-specific phagocytosis challenge, using E. coli coated-beads in control and 2-AG treated human microglia (a), shows that 2-AG (1 nM) treatment for 24 h significantly increases the internalization of these beads (b). RT-PCR analysis showing the enhanced expression of phagocytosis associated genes, *cd206*, *msr-1*, *sirp1α and trem2* in rat microglia treated with 2-AG (1 nM) for 6 h (c) and *trem2* for 24 h (d) relative to the vehicle-treated cells (dashed lines). Myelin isolated from the adult rat CNS was added to the microglia cultures for 6 h (e), showing that 2-AG enhances the expression of the phagocytosis associated genes, *cd206*, *msr-1*, and *lamp1* compared to control microglia. The proportion of the phagocytic microglia/field was also analyzed by immunocytochemistry 1 and 2 h after the addition of purified myelin for 24 h (f), in the presence of 2-AG (1 nM), TGF-β (20 ng/ml) or both, showing a temporary phagocytic response that is promoted by 2-AG and TGF-β administration. (g) No differences are found between microglia administered 2-AG and TGF-β when analyzing the phagocytic index of the cells. (h) The quantification of the Cy3-myelin internalized by microglia after 1 h of stimulation (i) shows a significant increase in myelin phagocytosis by 2-AG pretreatment via CB1 and CB2 receptors. Each point represents the mean ± SEM from: 4 microphotographs in 5 fields for human microglia ($^{*}p \leq 0.05$ *vs.* control); three to four independent experiments for RT-PCR studies ($^{*}p \leq 0.05$; $^{**}p \leq 0.01$, $^{***}p \leq 0.001$ *vs* control); four independent experiments for the phagocytosis assay ($^{**}p \leq 0.01$, $^{***}p \leq 0.001$ *vs* control; $^{\#}p \leq 0.05$ *vs.* 2-AG, $^{\#\#\#}p \leq 0.001$ *vs*. control at 1 h). Scale bar: 50 μm (a); 25 μm (i).

and OPCs also augments at 60 dpi relative to the vehicle TMEV mice. Hence, the direct effects of 2-AG on OPCs should be taken in consideration given that 2-AG promotes their proliferation (Gomez et al., 2015), survival and differentiation *in vitro* (Gomez et al., 2010, 2011).

The beneficial role of neuroinflammation in the reparative processes that take place in the CNS has been masked by the unquestionable immune-mediated pathology of MS and its animal models. The importance of microglia in remyelination can be summarized through three key effects: (i) the recruitment of progenitors, including stem cell populations; (ii) the secretion of cytokines, chemokines, growth factors and soluble mediators; and (iii) the efficient removal of debris at the lesion site (Napoli and Neumann, 2010). In the present work we found that corpus callosum demyelination was associated with OPC repopulation and it was followed by delayed microglial activation. Demyelination could be affecting the synthesis of pro-inflammatory cytokines, chemokines and growth factors as well as the eCB metabolic machinery. The relevance of TNFα and IL-1β in remyelination is supported by studies that show that the absence of these cytokines significantly delays remyelination (Arnett et al., 2001; Mason et al., 2001). These classical pro-inflammatory cytokines, together with CCL-2, can be synthesized by activated OPCs to enhance OPC mobilization into demyelinated areas (Moyon et al., 2015). Moreover, the reparative effects of TNF-α and IL-1β might be indirectly mediated by secondary mechanisms, since BDNF expression by astrocytes seems to be TNF-α dependent (Saha et al., 2006), and microglia and macrophages in IL-1β deficient mice fail to produce IGF-1 (Mason et al., 2001). In our study, the onset of remyelination in the corpus callosum of TMEV mice at 42 dpi was associated with increased *tnf-α* and *il-1β* gene expression, and that of *igf-1*, along with reduced *bdnf* gene expression, although this last change was counteracted and upregulated by 2-AG administration. Despite growth factors including BDNF promote oligodendrocyte differentiation and MBP expression (Dubois-Dalcq and Murray, 2000; Khorshidahmad et al., 2016) we cannot ensure that the effect of 2-AG on *bdnf* gene is contributing to the remyelination process that occurs in the corpus callosum. It is well established that long-term inflammation can be cytotoxic to OPCs (Setzu et al., 2006; Blakemore and Irvine, 2008) but the promoted microglia activation by 2-AG was followed in our study by a restoration of homeostasis, specifically in terms of the number and reactivity of microglia in the corpus callosum at 60 dpi, when complete remyelination was achieved.

Myelin debris is thought to impair remyelination and inhibit OPC differentiation (Kotter et al., 2006). Myelin contains inhibitory molecules that help establish a non-permissive environment (David and Lacroix, 2003; Schwab et al., 2005). Moreover, the direct contact of OPCs with CNS myelin inhibits their maturation in a concentration-dependent manner (Robinson and Miller, 1999). Indeed, blocking the clearance of myelin debris by microglia impairs remyelination (Lampron et al., 2015), such that an effective phagocytic response is needed after lesion for remyelination to occur. We found that there was a decrease in the expression of *sirp1α/cd47* in the demyelinated corpus callosum at 35 dpi, although this was subsequently restored to control levels at the onset of remyelination (42 dpi). It is likely that these changes are related to a specific increase in the phagocytosis of myelin debris following demyelination. The expression of phagocytosis associated genes was found to be quite variable, with less *mgf-e8* mRNA detected at 35 dpi, followed by an upregulation at 42 dpi. This could be related to the constant proportion of microglia with internalized MBP between the two time points, and a smaller volume of MBP phagocytosed at day 42 compared to 35 dpi.

The administration of 2-AG enhanced the expression of *msr1* at 35 dpi and *lamp1* at 42 dpi. We speculate that the mild changes of the phagocytic machinery following 2-AG treatment may be associated with intracellular myelin processing, as the aforementioned changes were accompanied by a boost in the proportion of microglial cells with internalized myelin from 35 to 42 dpi, together with the maintenance in the volume of MBP phagocytosed. Together, the *in vivo* analysis of phagocytosis suggests that 2-AG facilitated the clearance of myelin debris. In addition, 2-AG targeting rodent microglia cultures not only enhanced non-specific phagocytosis and the expression of most of the phagocytosis associated genes but also, the phagocytic capacity of purified myelin, augmenting myelin phagocytosis via the CB1 and CB2 cannabinoid receptors. This *in vitro* pro-phagocytic response of microglia to 2-AG might be related to the acquisition of an alternative activation state of microglia due to their own 2-AG synthesis. However, neither the balance between *nos-II/arg-1* genes nor their immunostaining was altered in the corpus callosum at 42 dpi. NOS-II and Arg-1 are two of the main markers used to identify classic and alternatively activated microglia, respectively (Mecha et al., 2015, 2018). The observation that cultured human microglia also enhances phagocytosis by 2-AG call into question the extent to which this finding is translatable to human microglia *in vivo*. The identity of the local cues from microenvironment that govern and shape microglia in the human adult brain remain largely unknown and constitutes an interesting field for future research.

We suggest that the modulation of microglia by 2-AG helps to establish the appropriate cellular and molecular milieu for OPCs thereby facilitating differentiation and the effective ensheathing of axons. This appropriate milieu includes moderate mRNA levels of pro-inflammatory cytokines, selective chemokines and growth factors, although their protein amounts should be assessed to verify this assumption. Indeed, alternatively activated microglia and macrophages drive OPC differentiation during remyelination when demyelination of the corpus callosum was induced by lysolecithin (Miron et al., 2013). Additional beneficial effects of enhanced eCB signaling should also be taken into account in our pathological paradigm, producing extensively documented anti-oxidant, anti-excitotoxic and neuroprotective effects that will also affect remyelination (Walter and Stella, 2004; Chiurchiú et al., 2018; Paloczi et al., 2017; Fernández-Ruiz et al., 2015).

Irrespective of the immunological processes that lead to demyelination, myelin debris is generated and must be efficiently removed to guarantee effective remyelination. The temporal discordance between OPC repopulation and the inflammation required for OPC activation leads to unsuccessful repair and thus, treatments designed to facilitate efficient remyelination would be predicted to protect neurons from axon degeneration, ameliorating subsequent clinical disability. Experimental models of demyelination have enabled factors that influence remyelination to be characterized. Consequently, some pro-remyelinating therapies have been tested in randomized controlled

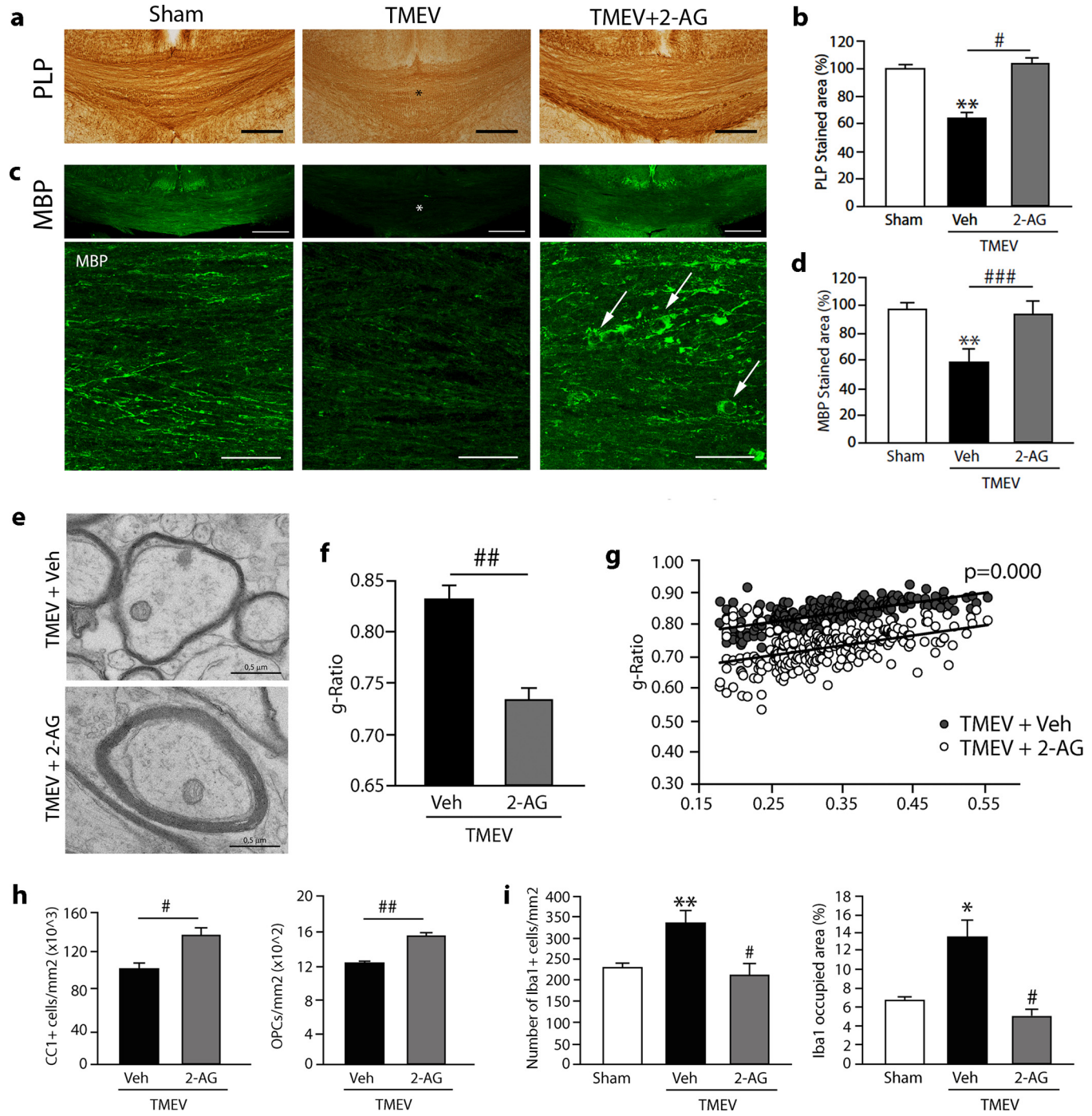

Fig. 7. 2-AG restores the myelin content in the corpus callosum and it increases the myelin thickness at 60 dpi. Immunohistochemistry of PLP (a) and MBP (c) in the corpus callosum at 60 dpi. Quantification shows that the PLP (b) and MBP (d) content is restored to Sham levels in mice administered 2-AG compared to those that received the vehicle alone. Ultrastructural analysis of myelin (e) reveals a lower g-Ratio in the corpus callosum of animals treated with 2-AG (f). (g), each symbol represents an axon and a p-value from the analysis of covariance (ANCOVA). At this time, 2-AG treated mice show an increase in the number of mature oligodendrocytes and OPCs (h), and resolution of the inflammatory process in terms of reduced number and reactivity of microglia (i). Each point represents the mean ± SEM from 6 mice per group of one to two independent experiments ($^{**}p \leq 0.01$ *vs.* Sham; $^{\#}p \leq 0.05$, $^{\#\#\#}p \leq 0.001$ *vs.* TMEV + Veh), and 3 mice in the TEM analysis ($^{\#\#}p \leq 0.01$ *vs.* TMEV + Veh). Scale bar: 500 µm (a, c), 25 µm in zoomed c; 0.5µm (e).

clinical trials, reporting some potential benefits (reviewed in Stangel et al. (2017)). The high expectations of these treatments contrast with the difficulty in accurately detecting demyelination and remyelination in patients using standard imaging technologies (Harlow et al., 2015). We propose that 2-AG administration couples OPC differentiation to the promotion of a beneficial microglial response that improved clearance of myelin debris, targeting multiple components of the myelination cascade. The results presented highlight the importance of integrating or engaging inflammatory and regenerative responses during the complex process of remyelination in future MS treatment paradigms.

Acknowledgements

We thank Laura Ramos, Nieves López and Martin Maher for their excellent technical support. This work was supported by grants from the Ministerio de Economía y Competitividad (MINECO SAF2013-42784-R,

SAF2016 76449-R), and the Red Española de Esclerosis Múltiple (REEM: RD12/0032/0008, RD16/0015/0021) sponsored by the Fondo de Investigación Sanitaria (FIS).

Competing interests.

The authors have no conflict of interests to declare.

Author contributions

MM and CG conceived and designed the experiments; MM, NYC, AF, FJCS, LM and IA performed the experiments; MM and NYC analyzed the data; MM wrote the paper; and CG and WY edited the manuscript.

Appendix A. Supplementary data

Supplementary data to this article can be found online at https://doi.org/10.1016/j.bbi.2018.12.013.

References

Ajami, B., Bennett, J.L., Krieger, C., McNagny, K.M., Rossi, F.M.V., 2011. Infiltrating monocytes trigger EAE progression, but do not contribute to the resident microglia pool. Nat. Neurosci. 14, 1142–1149.

Arévalo-Martín, A., Vela, J.M., Molina-Holgado, E., Borrell, J., Guaza, C., 2003. Therapeutic action of cannabinoids in a murine model of multiple sclerosis. J. Neurosci. 23 (7), 2511–2516.

Arnett, H.A., Mason, J., Marino, M., Suzuki, K., Matsushima, G.K., Ting, J.P., 2001. TNF alpha promotes proliferation of oligodendrocyte progenitors and remyelination. Nat. Neurosci. 4, 1116–1122.

Baer, A.S., Syed, Y.A., Kang, S.U., Mitteregger, D., Vig, R., Ffrench-Constant, C., Franklin, R.J., Altmann, F., Lubec, G., Kotter, M.R., 2009. Myelin-mediated inhibition of oligodendrocyte precursor differentiation can be overcome by pharmacological modulation of Fyn-RhoA and protein kinase C signalling. Brain 132 (Pt. 2), 465–481.

Bercury, K.K., Dai, J., Sachs, H.H., Ahrendsen, J.T., Wood, T.L., Macklin, W.B., 2014. Conditional ablation of raptor or rictor has differential impact on oligodendrocyte differentiation and CNS myelination. J. Neurosci. 34 (13), 4466–4480.

Bernal-Chico, A., Canedo, M., Manterola, A., Victoria Sánchez-Gómez, M., Pérez-Samartín, A., Rodríguez-Puertas, R., Matute, C., Mato, S., 2015. Blockade of monoacylglycerol lipase inhibits oligodendrocyte excitotoxicity and prevents demyelination in vivo. Glia 63 (1), 163–176.

Blakemore, W.F., 1974. Pattern of remyelination in the CNS. Nature 249 (457), 577–578.

Blakemore, W.F., Irvine, K.A., 2008. Endogenous or exogenous oligodendrocytes for remyelination. J. Neurol. Sci. 265, 43–46.

Boyd, A., Zhang, H., Williams, A., 2013. Insufficient OPC migration into demyelinated lesions is a cause of poor remyelination in MS and mouse models. Acta Neuropathol. 125 (6), 841–859.

Chang, A., Tourtellotte, W.W., Rudick, R., Trapp, B.D., 2002. Premyelinating oligodendrocytes in chronic lesions of multiple sclerosis. N. Engl. J. Med. 346 (3), 165–173.

Chari, D.M., 2007. Remyelination in multiple sclerosis. Int. Rev. Neurobiol. 79, 589–620.

Chari, D.M., Blakemore, W.F., 2002. Efficient recolonisation of progenitor-depleted areas of the CNS by adult oligodendrocyte progenitor cells. Glia 37 (4), 307–313.

Chiurchiù, V., Van der Stelt, M., Centonze, D., Maccarrone, M., 2018. The endocannabinoid system and its therapeutic exploitation in multiple sclerosis: clues for other neuroinflammatory diseases. Prog. Neurobiol. 160, 82–100.

Centonze, D., Bari, M., Rossi, S., Prosperetti, C., Furlan, R., Fezza, F., De Chiara, V., Battistini, L., Bernardi, G., Bernardini, S., et al., 2007. The endocannabinoid system is dysregulated in multiple sclerosis and in experimental autoimmune encephalomyelitis. Brain 130 (Pt. 10), 2543–2553.

Correa, F., Docagne, F., Mestre, L., Clemente, D., Henangómez, M., Loría, F., Guaza, C., 2009. A role for CB2 receptors in anandamide signalling pathways involved in the regulation of IL-12 and IL-23 in microglial cells. Biochem. Pharmacol. 77 (1), 86–100.

Croxford, J.L., Miller, S.D., 2003. Immunoregulation of a viral model of multiple sclerosis using the synthetic cannabinoid R+WIN55,212. J. Clin. Invest. 111 (8), 1231–1240.

David, S., Lacroix, S., 2003. Molecular approaches to spinal cord repair. Annu. Rev. Neurosci. 26, 411–440.

Di Marzo, V., Bifulco, M., De Petrocellis, L., 2004. The endocannabinoid system and its therapeutic exploitation. Nat. Rev. Drug Discov. 9, 771–784.

Dubois-Dalcq, M., Murray, K., 2000. Why are growth factors important in oligodendrocyte physiology? Pathol. Biol. 48 (1), 80–86.

Fife, B.T., Huffnagle, G.B., Kuziel, W.A., Karpus, W.J., 2000. CC chemokine receptor 2 is critical for induction of experimental autoimmune encephalomyelitis. J. Exp. Med. 192, 899–905.

Feliú, A., Moreno-Martet, M., Mecha, M., Carrillo-Salinas, F.J., de Lago, E., Fernández-Ruiz, J., Guaza, C., 2015. A Sativex(®)-like combination of phytocannabinoids as a disease-modifying therapy in a viral model of multiple sclerosis. Br. J. Pharmacol. 172 (14), 3579–3595.

Feliú, A., Bonilla Del Río, I., Carrillo-Salinas, F.J., Hernández-Torres, G., Mestre, L., Puente, N., Ortega-Gutiérrez, S., López-Rodríguez, M.L., Grandes, P., Mecha, M., et al., 2017. 2-Arachidonoylglycerol reduces proteoglycans and enhances remyelination in a progressive model of demyelination. J. Neurosci. 37 (35), 8385–8398.

Fernández-Ruiz, J., Romero, J., Ramos, J.A., 2015. Endocannabinoids and neurodegenerative disorders: Parkinson's disease, Huntington's chorea, Alzheimer's disease, and others. Handb. Exp. Pharmacol. 231, 233–259.

Franklin, R.J.M., Ffrench-Constant, C., 2008. Remyelination in the CNS: from biology to therapy. Nat. Rev. Neurosci. 9, 839–855.

Gitik, M., Liraz-Zaltsman, S., Oldenborg, P.A., Reichert, F., Rotshenker, S., 2011. Myelin down-regulates myelin phagocytosis by microglia and macrophages through interactions between CD47 on myelin and SIRPα (signal regulatory protein-α) on phagocytes. J. Neuroinflammation 8, 24.

Gomez, O., Arevalo-Martin, A., Garcia-Ovejero, D., Ortega-Gutierrez, S., Cisneros, J.A., Almazan, G., Sánchez-Rodriguez, M.A., Molina-Holgado, F., Molina-Holgado, E., 2010. The constitutive production of the endocannabinoid 2-arachidonoylglycerol participates in oligodendrocyte differentiation. Glia 58 (16), 1913–1927.

Gomez, O., Sanchez-Rodriguez, A., Le, M., Sanchez-Caro, C., Molina-Holgado, F., Molina-Holgado, E., 2011. Cannabinoid receptor agonists modulate oligodendrocyte differentiation by activating PI3K/Akt and the mammalian target of rapamycin (mTOR) pathways. Br. J. Pharmacol. 163 (7), 1520–1532.

Gomez, O., Sanchez-Rodriguez, M.A., Ortega-Gutierrez, S., Vazquez-Villa, H., Guaza, C., Molina-Holgado, F., Molina-Holgado, E., 2015. A basal tone of 2-arachidonoylglycerol contributes to early oligodendrocyte progenitor proliferation by activating phosphatidylinositol 3-kinase (PI3K)/AKT and the mammalian target of rapamycin (MTOR) pathways. J. Neuroimmune Pharmacol. 10 (2), 309–317.

Granja, A.G., Carrillo-Salinas, F.J., Pagani, A., Gómez-Cañas, M., Negri, R., Navarrete, C., Mecha, M., Mestre, L., Fiebich, B.L., Cantarero, I., et al., 2012. A cannabigerol quinone alleviates neuroinflammation in a chronic model of multiple sclerosis. J. Neuroimmune Pharmacol. 7 (4), 1002–1016.

Hanisch, U.K., Kettenmann, H., 2007. Microglia: active sensor and versatile effector cells in the normal and pathologic brain. Nat. Neurosci. 10 (11), 1387–1394.

Harlow, D.E., Honce, J.M., Miravalle, A.A., 2015. Remyelination therapy in multiple sclerosis. Front. Neurol. 6, 257.

Heppner, F.L., Greter, M., Marino, D., Falsig, J., RaivichG, Hövelmeyer N, Waisman, A., Rülicke, T., Prinz, M., Priller, J., et al., 2005. Experimental autoimmune encephalomyelitis repressed by microglial paralysis. Nat. Med. 11, 146–152.

Jurevics, H., Largent, C., Hostettler, J., Sammond, D.W., Matsushima, G.K., Kleindienst, A., Toews, A.D., Morell, P., 2002. Alterations in metabolism and gene expression in brain regions during cuprizone-induced demyelination and remyelination. J. Neurochem. 82, 126–136.

Khorshidahmad, T., Acosta, C., Cortes, C., Lakowski, T.M., Gangadaran, S., Namaka, M., 2016. Transcriptional regulation of brain-derived neurotrophic factor (BDNF) by methyl CpG binding protein 2 (MeCP2): a novel mechanism for re-myelination and/or myelin repair involved in the treatment of multiple sclerosis (MS). Mol. Neurobiol. 53 (2), 1092–1107.

Kocur, M., Schneider, R., Pulm, A.K., Bauer, J., Kropp, S., Gliem, M., Ingwersen, J., Goebels, N., Alferink, J., Prozorovski, T., et al., 2015. IFNβ secreted by microglia mediates clearance of myelin debris in CNS autoimmunity. Acta Neuropathol. Commun. 3, 20.

Kotter, M.R., Zhao, C., van Rooijen, N., Franklin, R.J.M., 2005. Macrophage-depletion induced impairment of experimental CNS remyelination is associated with a reduced oligodendrocyte progenitor cell response and altered growth factor expression. Neurobiol. Dis.

Kotter, M.R., Li, W.W., Zhao, C., Franklin, R.J.M., 2006. Myelin impairs CNS remyelination by inhibiting oligodendrocyte precursor cell differentiation. J. Neurosci. 26, 328–332.

Lampron, A., Larochelle, A., Laflamme, N., Préfontaine, P., Plante, M.M., Sánchez, M.G., Yong, V.W., Stys, P.K., Tremblay, M.È., Rivest, S., 2015. Inefficient clearance of myelin debris by microglia impairs remyelinating processes. J. Exp. Med. 212, 481–495.

Larocca, J.N., Norton, W.T., 2007. Isolation of myelin. In: Curr. Protoc. Cell Biol. pp. 25 (Chapter 3 Unit 3).

Lledó, A., Borrell, J., Guaza, C., 1999. Dexamethasone regulation of interleukin-1-receptors in the hippocampus of Theiler's virus-infected mice: effects on virus-mediated demyelination. Eur. J. Pharmacol. 372 (1), 75–83.

Lourbopoulos, A., Grigoriadis, N., Lagoudaki, R., Touloumi, O., Polyzoidou, E., Mavromatis, I., Tascos, N., Breuer, A., Ovadia, H., Karussis, D., et al., 2011. Administration of 2-arachidonoylglycerol ameliorates both acute and chronic experimental autoimmune encephalomyelitis. Brain Res. 1390, 126–141.

Ludwin, S.K., Maitland, M., 1984. Long-term remyelination fails to reconstitute normal thickness of central myelin sheaths. J. Neurol. Sci. 64 (2), 193–198.

Manterola, A., Bernal-Chico, A., Cipriani, R., Canedo-Antelo, M., Moreno-García, A., Martín-Fontecha, M., Pérez-Cerdá, F., Sánchez-Gómez, M.V., Ortega-Gutiérrez, S., Brown, J.M., Hsu, K.L., Cravatt, B., Matute, C., Sato, S., 2018. Deregulation of the endocannabinoid system and therapeutic potential of ABHD6 blockade in the cuprizone model of demyelination. Biochem. Pharmacol (Epub ahead of print).

Mason, J.L., Suzuki, K., Chaplin, D.D., Matsushima, G.K., 2001. Interleukin-1beta promotes repair of the CNS. J. Neurosci. 21 (18), 7046–7052.

McCarthy, K.D., De Vellis, J., 1980. Preparation of separate astroglial and oligodendroglial cell cultures from rat cerebral tissue. J. Cell Biol. 85, 890–902.

Mecha, M., Carrillo-Salinas, F.J., Mestre, L., Feliú, A., Guaza, C., 2013a. Viral models of multiple sclerosis: neurodegeneration and demyelination in mice infected with Theiler's virus. Prog. Neurobiol. 101–102, 46–64.

Mecha, M., Feliú, A., Carrillo-Salinas, F.J., Mestre, L., Guaza, C., 2013b. Mobilization of progenitors in the subventricular zone to undergo oligodendrogenesis in the Theiler's virus model of multiple sclerosis: implications for remyelination at lesion sites. Exp. Neurol. 250, 348–352.

Mecha, M., Feliú, A., Carrillo-Salinas, F.J., Rueda-Zubiaurre, A., Ortega-Gutiérrez, S., de Sola, R.G., Guaza, C., 2015. Endocannabinoids drive the acquisition of an alternative

phenotype in microglia. Brain Behav. Immun. 49, 233–245.
Mecha, M., Feliú, A., Machín, I., Cordero, C., Carrillo-Salinas, F.J., Mestre, L., Hernández-Torres, G., Ortega-Gutiérrez, S., López-Rodríguez, M.L., de Castro, F., et al., 2018. 2-AG limits Theiler's virus induced acute neuroinflammation by modulating microglia and promoting MDSCs. Glia 66 (7), 1447–1463.
Mei, F., Wang, H., Liu, S., Niu, J., Wang, L., He, Y., Etxeberria, A., Chan, J.R., Xiao, L., 2013. Stage-specific deletion of Olig2 conveys opposing functions on differentiation and maturation of oligodendrocytes. J. Neurosci. 33 (19), 8454–8462.
Mestre, L., Iñigo, P.M., Mecha, M., Correa, F.G., Hernangómez-Herrero, M., Loría, F., Docagne, F., Borrel, J., Guaza, C., 2011. Anandamide inhibits Theiler's virus induced VCAM-1 in brain endothelial cells and reduces leukocyte transmigration in a model of blood brain barrier by activation of CB(1) receptors. J. Neuroinflammation. 2011 (8), 102.
Miron, V.E., Kuhlmann, T., Antel, J.P., 2011. Cells of the oligodendroglial lineage, myelination, and remyelination. BBA 1812 (2), 184–193.
Miron, V.E., Boyd, A., Zhao, J.W., Yuen, T.J., Ruckh, J.M., Shadrach, J.L., van Wijngaarden, P., Wagers, A.J., Williams, A., Franklin, R.J.M., et al., 2013. M2 microglia and macrophages drive oligodendrocyte differentiation during CNS remyelination. Nat. Neurosci. 16 (9), 1211–1218.
Molina-Holgado, E., Vela, J.M., Arévalo-Martín, A., Guaza, C., 2001. LPS/IFN-gamma cytotoxicity in oligodendroglial cells: role of nitric oxide and protection by the anti-inflammatory cytokine IL-10. Eur. J. Neurosci. 13 (3), 493–502.
Moyon, S., Dubessy, A.L., Aigrot, M.S., Trotter, M., Huang, J.K., Dauphinot, L., Potier, M.C., Kerninon, C., Melik Parsadaniantz, S., Franklin, R.J.M., et al., 2015. Demyelination causes adult CNS progenitors to revert to an immature state and express immune cues that support their migration. J. Neurosci. 35 (1), 4–20.
Napoli, I., Neumann, H., 2010. Protective effects of microglia in multiple sclerosis. Exp. Neurol. 225, 24–28.
Natrajan, M.S., Komori, M., Kosa, P., Johnson, K.R., Wu, T., Franklin, R.J.M., Bielekova, B., 2015. Pioglitazone regulates myelin phagocytosis and multiple sclerosis monocytes. Ann. Clin. Transl. Neurol. 2 (12), 1071–1084.
Nave, K.A., 2010. Myelination and support of axonal integrity by glia. Nature 468 (7321), 244–252.
Neumann, H., Kotter, M.R., Franklin, R.J.M., 2009. Debris clearance by microglia: an essential link between degeneration and regeneration. Brain 132, 288–295.
Nuttall, R.K., Silva, C., Bar-Or, A., Patel, K., Edwards, D.R., Yong, V.W., 2007. Metalloproteinases (MMPs and ADAMs) are enriched in microglia compared to leukocytes and they link microglia activation with cytokine levels. Glia 55, 516–526.
Olah, M., Amor, S., Brouwer, N., Vinet, J., Eggen, B., Biber, K., Boddeke, H.W., 2012. Identification of a microglia phenotype supportive of remyelination. Glia 60, 306–321.
Oleszak, E.L., Chang, J.R., Friedman, H., Katsetos, C.D., Platsoucas, C.D., 2004. Theiler's virus infection: a model for multiple sclerosis. Clin. Microbiol. Rev. 17 (1), 174–207.
Ortega-Gutiérrez, S., Molina-Holgado, E., Arévalo-Martín, A., Correa, F., Viso, A., López-Rodríguez, M.L., Di Marzo, V., Guaza, C., 2005. Activation of the endocannabinoid system as therapeutic approach in a murine model of multiple sclerosis. FASEB J. 19 (10), 1338–1340.
Paloczi, J., Varga, Z.V., Hasko, G., Pacher, P., 2017. Neuroprotection in oxidative stress-related neurodegenerative diseases: role of endocannabinoid system modulation. Antioxid. Redox Signal. 29 (1), 75–108.
Pacher, P., Bátkai, S., Kunos, G., 2006. The endocannabinoid system as an emerging target of pharmacotherapy. Pharmacol. Rev. 58 (3), 389–462.
Patel, J.R., Klein, R.S., 2011. Mediators of oligodendrocyte differentiation during remyelination. FEBS Lett. 585 (23), 3730–3737.
Plemel, J.R., Liu, W.Q., Yong, V.W., 2017. Remyelination therapies: a new direction and challenge in multiple sclerosis. Nat. Rev. Drug Discov. 16 (9), 617–634.
Prineas, J.W., Barnard, R.O., Kwon, E.E., Sharer, L.R., Cho, E.S., 1993. Multiple sclerosis: remyelination of nascent lesions. Ann. Neurol. 33 (2), 137–151.
Robinson, S., Miller, R.H., 1999. Contact with central nervous system myelin inhibits oligodendrocyte progenitor maturation. Dev. Biol. 216 (1), 359–368.
Saha, R.N., Liu, X., Pahan, K., 2006. Up-regulation of BDNF in astrocytes by TNF-alpha: a case for the neuroprotective role of cytokine. J. Neuroimmune Pharmacol. 1 (3), 212–222.
Schwab, J.M., Failli, V., Chédotal, A., 2005. Injury-related dynamic myelin/oligodendrocyte axon-outgrowth inhibition in the central nervous system. Lancet 365 (9476), 2055–2057.
Setzu, A., Lathia, J.D., Zhao, C., Wells, K., Rao, M.S., Ffrench-Constant, C., Franklin, R.J.M., 2006. Inflammation stimulates myelination by transplanted oligodendrocyte precursor cells. Glia 54 (4), 297–303.
Southwick, P.L., Ernst, L.A., Tauriello, E.W., Parker, S.R., Mujumdar, R.B., Mujumdar, S.R., Clever, H.A., Waggoner, A.S., 1990. Cyanine dye labeling reagents–carboxymethylindocyanine succinimidyl esters. Cytometry 11 (3), 418–430.
Stangel, M., Kuhlmann, T., Matthews, P.M., Kilpatrick, T.J., 2017. Achievements and obstacles of remyelinating therapies in multiple sclerosis. Nat. Rev. Neurol. 13 (12), 742–754.
Streit, W.J., Conde, J.R., Fendrick, S.E., Flanary, B.E., Mariani, C.L., 2005. Role of microglia in the central nervous system's immune response. Neurol. Res. 27 (7), 685–691.
Tsunoda, I., Fujinami, R.S., 2010. Neuropathogenesis of Theileŕs murine encephalomyelitis virus infection, an animal model for multiple sclerosis. J. Neuroimmune Pharmacol. 5 (3), 355–369.
Walter, L., Stella, N., 2004. Cannabinoids and neuroinflammation. Br. J. Pharmacol. 141 (5), 775–785.